PHYSICAL REVIEW D VOLUME 19, NUMBER 9 1 MAY 1979

Hadron production in muon-proton and muon-deuteron collisions

W. A. Loomis, B. A. Gordon, F. M. Pipkin, S. H. Pordes,* W. D. Shambroom, L. J. Verhey,† and Richard Wilson
High Energy Physics Laboratory and Department of Physics, Harvard University, Cambridge, Massachusetts 02138

H. L. Anderson, R. M. Fine,‡ R. H. Heisterberg,§ H. S. Matis,‖ L. Mo,§ L. C. Myrianthopoulos, and S. C. Wright
Enrico Fermi Institute, University of Chicago, Chicago, Illinois 60637

W. R. Francis,¶ R. G. Hicks, and T. B. W. Kirk**
Department of Physics, University of Illinois, Urbana, Illinois 61801

V. K. Bharadwaj,†† N. E. Booth, G. I. Kirkbride,‡‡ T. W. Quirk, A. Skuja,§§ M. A. Staton, and W. S. C. Williams
Nuclear Physics Laboratory, Oxford University, Keble Road, Oxford OX1, 3RH, England
(Received 25 October 1977; revised manuscript received 13 November 1978)

This paper reports measurements of the hadrons produced in the inelastic scattering of 147-GeV muons by protons and deuterons in an experiment carried out at Fermi National Accelerator Laboratory. Both the scattered muon and the hadrons were measured in a large spectrometer. Properties of the hadron spectra are presented for proton, deuteron, and neutron targets and compared with theoretical models and with hadron spectra from related processes. Emphasis is placed on the quark-parton model and the data are found to be in substantial agreement with it. The average transverse momentum of the hadrons with respect to the virtual photon direction shows no dependence on the muon scattering variables. The data display "jet behavior" of the inclusive hadrons comparable to that found in e^+e^- annihilations.

I. INTRODUCTION

The discovery[1] at the Stanford Linear Accelerator Center of approximate "scaling" in the inelastic scattering of electrons by nucleons opened a fruitful area of research. Because of the smallness of the fine-structure constant, α, it had long been appreciated that, if radiative corrections were ignored, the description of electron and muon scattering could be well approximated by the single graph shown in Fig. 1. In this approximation the total inelastic lepton cross section can be interpreted in terms of two nucleon structure functions.

The surprise of "scaling" was that at high momentum transfers the structure functions did not depend directly on the two Lorentz invariants that define the scattering process (Q^2 and ν), but only on the ratio $\omega = 2M\nu/Q^2$. Bjorken[2] had pointed out earlier that such a situation could arise from consideration of the commutation properties of the electromagnetic current; as a result this behavior is called Bjorken scaling. Stimulated by the SLAC data, Feynman[3] and others[4] proposed a simpler explanation in terms of pointlike constituents of the nucleons, called partons. Since these simple explanations of "scaling" predicted that the data would continue to scale as Q^2 and ν increased, it was important to continue the measurements begun at SLAC at the higher energies available at Fermilab. Another compelling direction for further research was investigation of the properties of the hadrons produced by the inelastically scattered lepton. It was hoped that these properties would yield further insight into the constituents of the nucleon.

A series of muon scattering experiments was performed at Fermilab to further these investigations. Muons rather than electrons were used since they were more readily available at Fermilab and since they are essentially heavy electrons by all tests.[5] Another advantage of muons is that the radiative corrections are smaller. The experiment was designed to look at both the scattered muon and the hadron final state. An order-of-magnitude increase in beam energy over that of previous SLAC measurements as well as a doubling of the momentum-transfer-squared interval was achieved.

This paper describes the properties of the inclusive hadron distributions measured in the initial series of experiments. Some of this work has been published in letters[6,7] and was the basis for the Ph.D. thesis of Matis.[8] Companion publications[9,10] and the theses of Bharadwaj,[11] Gordon,[12] Kirkbride,[13] and Pordes[14] cover the inclusive muon scattering and give more detail on the apparatus and some aspects of the analysis. An independent

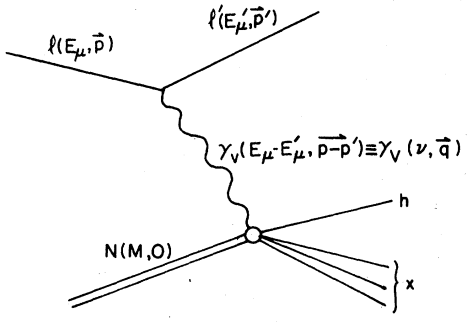

FIG. 1. Feynman graph for muon scattering by one photon exchange.

analysis of the muon inclusive scattering and hadron distributions for the deuterium data is given in the thesis of Heisterberg.[15]

II. KINEMATICS

In the single-photon-exchange approximation the discussion of hadron production in lepton scattering can be reduced to a discussion of photon-hadron interactions, where the photon is the exchanged virtual photon. As depicted schematically in Fig. 1, the lepton scatters from the nucleon by exchanging the virtual photon. Thus muoproduction can be treated as the virtual-photoproduction reaction

$$\gamma_v + N \rightarrow \text{hadrons}. \tag{1}$$

In this paper we are particularly concerned with inclusive reactions where a single hadron is studied. In terms of the kinematic variables defined in Fig. 1 and Table I, the muoproduction cross section for inelastic hadron production can be written in the form

$$\frac{d^5\sigma}{dQ^2 ds dp^3} = \frac{\pi}{2ME_\mu E'_\mu}\Gamma\frac{d^3s}{dp^3}, \tag{2}$$

where

$$\Gamma = \frac{\alpha}{2\pi^2}\frac{(s-M^2)}{MQ^2}\left(\frac{1}{1-\epsilon}+\frac{2m\mu^2}{Q^2}\right) \tag{3}$$

and

$$\epsilon = \left[1+2\frac{(Q^2+\nu^2)}{\beta Q^2}\tan^2(\tfrac{1}{2}\theta)\right]^{-1}. \tag{4}$$

Here

$$\beta = (1 - Q^2_{\min}/Q^2)^2. \tag{5}$$

Γ is the usual flux of virtual photons per incident muon, and ϵ is the polarization parameter for the virtual photons. In addition to the transverse polarization characteristic of real photons, the virtual photon has a longitudinal component whose magnitude depends upon ϵ. The inclusive hadron virtual-photoproduction cross section can be expressed in the form

$$\frac{d^3\sigma}{dp^3} = \frac{d\sigma_t}{dp^3} + \epsilon\frac{d\sigma_s}{dp^3} + \epsilon\frac{d\sigma_{tt}}{dp^3}\cos 2\phi + \left[\frac{\epsilon(\epsilon+1)}{2}\right]^{1/2}\frac{d\sigma_{ts}}{dp^3}\cos\phi, \tag{6}$$

where ϕ is the angle between the muon scattering plane and the hadron production plane. The four cross sections in Eq. (6) are the contributions from transverse photons, longitudinal photons, the interference of the transverse amplitudes, and the interference of the longitudinal and transverse amplitudes. While it is not necessary to describe the final-state hadrons in terms of the interaction of a beam of virtual photons with nucleons, it is convenient because it allows direct and simple comparisons of these results with those obtained in real-photon–nucleon scattering and in hadron-hadron scattering.

For most of the data we have used kinematic variables defined either in the laboratory system or in the virtual-photon–nucleon center-of-mass system. A final-state hadron in the virtual-photon–nucleon center-of-mass system is defined by its energy E^* and its momentum p^* (see Fig. 2). Hadron spectra are usually described in terms of the Lorentz-invariant cross section:

TABLE I. Definition of kinematic variables for the reaction $\mu + p \rightarrow \mu + h +$ anything.

m_μ	Muon mass
E_μ	Incident muon energy
E'_μ	Scattered muon energy
θ_μ	Muon scattering angle
ν	Virtual-photon laboratory energy
Q^2	Virtual-photon negative mass squared
ϵ	Virtual-photon polarization parameter
s	Square of virtual-photon–target-nucleon system center-of-mass energy
E^*	Hadron energy in virtual-photon–target-nucleon center-of-mass system
E	Hadron energy in the lab system
p^*	Hadron momentum in virtual-photon–target-nucleon center-of-mass system
p	Hadron momentum in the laboratory system
p_T	Hadron momentum transverse to virtual-photon direction
M	Nucleon mass
ϕ	Azimuthal angle of hadron about virtual photon referenced to scattering plane of muon
t	Four-momentum transfer squared to target nucleon

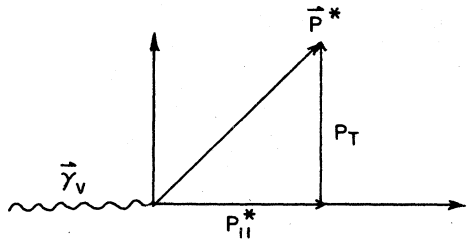

FIG. 2. Hadron kinematics in the photon-nucleon center-of-mass frame.

$$E^* \frac{d^3\sigma}{dp^{*3}}. \tag{7}$$

On occasion we use the cross section

$$\frac{d^3\sigma}{dp^{*3}} \tag{8}$$

whose integral

$$\int dp^{*3} \frac{d^3\sigma}{dp^{*3}} = \langle n \rangle \sigma \tag{9}$$

is also an invariant. Here $\langle n \rangle$ is the average multiplicity for the hadrons, and σ is the total cross section for an interaction. The invariant cross section, Eq. (7), has simple representations in terms of hadron variables less cumbersome than the momentum in a particular frame of reference. A hadron is defined by its momentum transverse to the direction of the virtual photon, p_T, and by a variety of longitudinal variables. The most important of these is the scaled longitudinal momentum:

$$x' = \frac{p_{\parallel}^*}{(p_{\max}{}^{*2} - p_T{}^2)^{1/2}} \simeq \frac{2p_{\parallel}^*}{\sqrt{s}} = x. \tag{10}$$

$p_{\parallel}^*$ is the longitudinal momentum of the hadron and $p_{\max}^*$ is the maximum momentum the hadron can have in the virtual-photon–target-nucleon center-of-mass frame. The use of the symbol x, which is commonly referred to as Feynman x, is unfortunate because of its common usage in the literature of inelastic lepton scattering as the Bjorken scaling variable $x = 1/\omega = Q^2/2M\nu$. To avoid confusion we will use x_B for the Bjorken x.

The rapidity y is defined with respect to an axis z as

$$y = \frac{1}{2} \ln \frac{E^* + p_{\parallel}^*}{E^* - p_{\parallel}^*} = \frac{1}{2} \ln \frac{1 + \beta_z}{1 - \beta_z}, \tag{11}$$

where $\beta_z = p_{\parallel}^*/E^*$. The difference between the rapidity of two particles is invariant under a Lorentz transformation along the z axis. Rapidity is thus a useful variable for looking at correlations among the final-state hadrons. The rapidity interval between particles is an indication of how each hadron "sees" the others in an inertial frame in which its velocity is zero along the z axis. This usefulness is enhanced because the average transverse momentum of hadrons is small compared to the maximum possible and has only weak dependence on other kinematic variables. The boundaries of rapidity phase space depend on the center-of-mass energy. Since the virtual-photon beam has a broad band of energies and since we are mainly interested in hadrons with a large fraction of the virtual photon's momentum, we use rapidity relative to the maximum possible rapidity for a produced pion,

$$\Delta y = y_{\max} - y. \tag{12}$$

Another useful hadron variable is the invariant

$$z = E/\nu, \tag{13}$$

whose value lies between 0 and 1. The value of x' by comparison lies between -1 and $+1$. z and x' are used interchangeably in the description of hadron production since for z or x' greater than 0.15, they are almost equal for the typical hadrons observed. Note that while z is a Lorentz

TABLE II. Expressions for $(E/\sigma)(d^3\sigma/dp^3)$.

Variables	Formula	Approx. formula with limits
x', p_T	$\frac{1}{\pi\sigma} \frac{E^*}{(p_{\max}{}^{*2} - p_T{}^2)^{1/2}} \frac{d^2\sigma}{dx' dp_T{}^2}$	$\frac{x'}{\pi\sigma} \frac{d^2\sigma}{dx' dp_T{}^2}$, $p_{\parallel} \gg p_T$
$x' = \frac{p_{\parallel}^*}{(p_{\max}{}^{*2} - p_T{}^2)^{1/2}}$		
$\Delta y, p_T$	$\frac{1}{\pi\sigma} \frac{d^2\sigma}{d\Delta y dp_T{}^2}$	
$\Delta y = y_{\max} - y$		
$y = \frac{1}{2} \ln\left(\frac{E + p_{\parallel}}{E - p_{\parallel}}\right)$		

TABLE III. Integrals of $(E/\sigma)(d^3\sigma/dp^3)$ and $(1/\sigma)(d^3\sigma/dp^3)$.

Name	Definition	Approximate formula
Longitudinal structure function	$F(x')=\int_0^{p_{T\max}{}^2} dp_T{}^2 \frac{E}{\sigma}\frac{d^3\sigma}{dp^3}(x',p_T{}^2)$	$F(x')\cong\frac{x'}{\pi\sigma}\frac{d\sigma}{dx'}$, $x'>0.15$
z structure function	$F(z)=\frac{z}{\pi\sigma}\frac{d\sigma}{dz}$	$F(z)=\frac{z}{\pi\sigma}\frac{d\sigma}{dz}$
Rapidity structure function	$F(\Delta y)=\int_0^{p_{T\max}{}^2} dp_T{}^2 \frac{E}{\sigma}\frac{d^3\sigma}{dp^3}(\Delta y,p_T{}^2)$	$F(\Delta y)=\frac{1}{\pi\sigma}\frac{d\sigma}{d\Delta y}$
Partial multiplicity	$N(x_1',x_2')=\int_0^{p_{T\max}{}^2}\int_{x_1'}^{x_2'} dx'\frac{1}{\sigma}\frac{d^3\sigma}{dx'dp_T{}^2}(x',p_T{}^2)$	
Moments of transverse momentum	$\langle p_T{}^n\rangle(x_1',x_2')=\frac{\int_{x_1'}^{x_2'}dx'\int_0^{p_{T\max}{}^2}dp_T{}^2\lvert p_T\rvert^n\frac{d^3\sigma}{dp^3}(x',p_T{}^2)}{\int_{x_1'}^{x_2'}dx'\int_0^{p_{T\max}{}^2}dp_T{}^2\frac{d^3\sigma}{dp^3}(x',p_T{}^2)}$	

invariant, x' distinguishes between hadronic fragments of the target nucleon and hadron fragments of the photon. A fragment is a particle having a substantial fraction, 10% or more, of the initial longitudinal center-of-mass momentum of the nucleon or photon.

Most of the data are presented in terms of the invariant structure function

$$\frac{E^*}{\sigma}\frac{d^3\sigma}{dp^{*3}}. \tag{14}$$

Here σ is the total virtual-photoproduction cross section. The invariant structure function gives, in effect, the number of hadrons per interacting muon rather than per incident muon and suppresses the Q^2 and ν dependence of the muon inclusive cross section. Table II summarizes expressions for the invariant structure function in terms of the variables defined above. Table III defines integrals of the structure function that will be used in the discussion of results. In most cases the results are presented in terms of the ϕ-averaged structure function.

The most important integral of the invariant structure function is the ϕ-averaged longitudinal structure function defined by

$$F(x')=\frac{1}{2\pi}\int_0^{p_{T\max}{}^2} dp_T{}^2\int_0^{2\pi} d\phi\frac{E^*}{\sigma}\frac{d^3\sigma}{dp^{*3}} \tag{15}$$

$$\simeq\frac{x'}{\pi\sigma}\frac{d\sigma}{dx'},\quad (x'>0.15). \tag{16}$$

III. THEORY

This section outlines the predictions of some of the theoretical models relevant to production of hadrons by muons. In the important case of the quark-parton model we have briefly described the model since it is simple and widely used.

A. The quark-parton model

The quark-parton model views all hadrons as bound states of more elementary pointlike charged particles called partons. Strong interactions bind the partons together. Muon and electron scattering from nucleons take place through elastic collisions between the muon or electron and partons which carry momentum equal to a fraction x_B of the momentum of the nucleon. Scaling is a consequence of the pointlike nature of the parton and the fact that the partons act like independent particles during the scattering. In this simple picture $\nu W_2(x_B)$ is the momentum-weighted distribution function of the partons in the nucleon. That is,

$$\nu W_2(x_B)=x_B\sum_i q_i{}^2 f_i(x_B), \tag{17}$$

where the summation is taken over the partons in the nucleon, q_i is the charge of the ith parton, and $f_i(x_B)$ is the momentum distribution for the ith parton.

In the interaction the struck parton is separated in phase space from its original partners and it fragments into hadrons largely independently of them. This behavior is depicted schematically in Fig. 3. The hadronic structure function $F(x')$

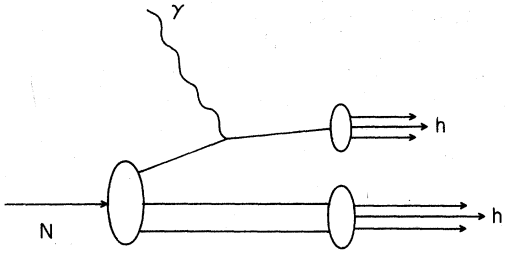

FIG. 3. Schematic of virtual-photon interactions according to the parton model.

is then given by

$$F^{\pm}(x', x_B) = \frac{\sum_i q_i^2 f_i(x_B) D_i^{\pm}(x')}{\sum_i q_i^2 f_i(x_B)}, \tag{18}$$

where $D_i^{\pm}(x')$ is the distribution function giving the probability for a parton of type i to produce a positive or negative hadron with a fractional momentum x'. Thus, the quark-parton model predicts that $F(x')$ depends on Q^2 and ν only through the parameter x_B.

If we specialize the model to the u, d, and s quarks we can make more specific predictions. For this discussion we will lump the newer quarks such as charm under the designation s. Charge-conjugation invariance among the quarks implies

$$D_u^+(x') = D_{\bar{u}}^-(x'), \tag{19}$$

and, assuming that u and d quarks fragment only into pions, isospin invariance gives

$$D_u^+(x') = D_{\bar{d}}^-(x'). \tag{20}$$

In this case

$$F(x') = \frac{\frac{4}{9}(D_u^{\pm} f_u + D_{\bar{d}}^{\pm} f_{\bar{u}}) + \frac{1}{9}(D_{\bar{d}}^{\pm} f_{\bar{d}} + D_u^{\pm} f_{\bar{d}}) + \frac{1}{9}(D_s^{\pm} f_s + D_{\bar{s}}^{\pm} f_{\bar{s}})}{\frac{4}{9}(f_u + f_{\bar{u}}) + \frac{1}{9}(f_{\bar{d}} + f_d) + \frac{1}{9}(f_s + f_{\bar{s}})}. \tag{21}$$

If we assume f_s and $f_{\bar{s}}$ are small and neglect them

$$F^+(x') + F^-(x') = D_u^+(x') + D_u^-(x'). \tag{22}$$

Thus, we expect the average of the positive and negative structure functions to be independent of x_B according to this model.

Neutrino reactions should produce hadrons according to the same rules. If the amounts of s quarks and antiquarks in the nucleon are small, neutrinos will interact only with the u quark and antineutrinos with the d quark. Thus

$$\begin{aligned} F_{\nu p}^+ &= D_u^+(x'), \\ F_{\nu p}^- &= D_u^-(x'). \end{aligned} \tag{23}$$

We would have then

$$F_{\gamma_\nu p}^+ + F_{\gamma_\nu p}^- = F_{\nu p}^+ + F_{\nu p}^-. \tag{24}$$

The hadron charge ratio N^+/N^- is defined:

$$N^+/N^- = \frac{N^+(x_1', x_2')}{N^-(x_1', x_2')}, \tag{25}$$

where $N^{\pm}(x_1', x_2')$ are the partial multiplicities listed in Table III. Dakin and Feldman[16] have shown that in the quark model N^+/N^- can be expressed in terms of the quark distribution function $f_i(x_B)$ and $\eta(x')$, where $\eta(x')$ is the charge ratio for a beam of pure u quarks.

$$\eta(x') = \frac{D_u^+(x')}{D_u^-(x')}. \tag{26}$$

If η is assumed to be independent of x', then the charge ratio will depend only on x_B. The measurements are not inconsistent with the expectations of this quark model.

The azimuthal distribution of hadrons about the virtual-photon direction may be described in the one-photon approximation by Eq. (6). Ravndal[17] has shown that in a simple model where the partons have spin $\frac{1}{2}$ and one ignores gluon effects the coefficients of $\cos\phi$ and $\cos 2\phi$ in Eq. (6) are expected to be small and to vanish with increasing Q^2.

The asymptotically free gauge theories (AFGT) expand the parton model into renormalizable theories. Gluons are postulated to bind the quarks together in a fashion similar to that of photons in quantum electrodynamics. These theories have been quite successful in explaining the scaling violations observed in muon inclusive scattering.[18] They can also predict some features of muoproduced hadrons. In the simple parton model already discussed, the average transverse momentum squared of hadrons about the virtual-photon direction should be the sum of that initially carried by the struck parton and the transverse momentum squared inherent in the fragmentation process. The observed transverse momentum might be expected to be a function only of x_B and z (aside from radiative corrections). The prediction of AFGT is that the average transverse momentum of hadron fragments should increase with Q^2 at fixed x_B.[19] The resultant violation of x_B scaling is a natural outcome of the same processes that cause scale violation in muon inclusive scattering.

Clearly, the parton model and its extensions can make detailed predictions. We refer the reader to the recent work of Feynman, Field, and Fox[20] for more comprehensive discussions.

B. Jets

Many individuals have predicted the existence of jets.[21] The concept arises from the necessary

fragmentation of partons into hadrons (partons are not observed) and the fact that in most interactions final-state hadrons have limited transverse momentum with respect to some axis—usually that of the incident particles. It is hypothesized that the hadrons from a fragmenting parton have low momentum in the partons' rest frame and therefore low transverse momentum to the partons' direction in any frame. The hadron fragments of a single parton that is well isolated kinematically from other partons in a interaction will appear in a collimated jet. This idea has been controversial mainly because it is hard to make a precise definition of jet properties. It is difficult to make the definition Lorentz invariant.

Despite this problem there is good evidence for the existence of jets in electron-positron annihilation.[22] The parton model predicts that the electron and positron annihilate into a parton and an antiparton which then fragment into back-to-back hadron jets. At high center-of-mass energies, hadronic annihilation events show a sphericity[23] distribution that is expected from jet production as opposed to that for isotropic production of hadrons. There are in effect more events in which the particles are collimated along a single axis than isotropic production would predict.

Insofar as parton-fragmentation jets exist they should be observed along the direction of the virtual photon in muoproduction. Although the distribution of quark types produced or ejected is different in annihilation and muoproduction, the expectation is that the gross properties of the hadron distribution about the jet axis would be the same.

C. Hadronic aspects of photons

The photon has long been thought to have a hadronic component leading to hadronlike behavior. Bauer, Spital, Yennie, and Pipkin[24] have recently reviewed the body of theory and experiment on this subject. With this point of view it is natural to examine virtual-photon–produced hadrons to see if well known features of hadron-hadron scattering such as Feynman scaling[25] occur in this case as well.

A more specific suggestion based on the hadronic nature of the photon was made first by Wu and Cheng.[26] Motivated by the results obtained in quantum-electrodynamic calculations, they suggested that the effective transverse size of the virtual photon might decrease with the mass of the virtual photon like $(1/Q^2)^{1/2}$. As a consequence they suggested that all t distributions in ρ production by virtual photons would become less steep as Q^2 increased. The data[27] give some evidence for the predicted change in the elastic t distributions in ρ production from hydrogen. In conjunction with the uncertainty principle, the space-time picture of the photon suggests that the average transverse momentum of the muoproduced hadrons must increase with Q^2.

IV. EXPERIMENTAL APPARATUS

The apparatus used in this study is shown schematically in Fig. 4. The incident muon beam struck the hydrogen or deuterium target and scattered muons triggered the apparatus. The triggering was done by the scintillation-counter electronic-coincidence technique. The counters B signalled the presence of an incoming beam muon. The counters V vetoed triggers where a halo muon (a muon moving along with, but not in, the beam) was present. A muon which scattered through a large-enough angle or lost sufficient energy counted in G, M, and M', and was absent from the beam veto N. The event trigger was then the coincidence $B \cdot (\overline{V+N}) \cdot G \cdot (M+M')$. Upon the occurrence of an event, triggering was suspended, "live-time" scalers were halted, all counter discriminators and set wires in the proportional chambers were latched and the spark chambers were triggered. Some 20 μsec later when all spark noise had died down, counter bits, scaler information, addresses of sparks and set wires were read in and recorded on tape by a Xerox Σ-3 computer. Subsequently, the apparatus was reset and armed for the next event.

Particle trajectories were specified by information read in from wire spark and proportional chambers. The incident beam was measured before and after the dipoles (1E4) by six, 20-cm square multiwire proportional chambers with 2-mm wire spacing (S0). These measurements determined the transverse position (to ±1mm)

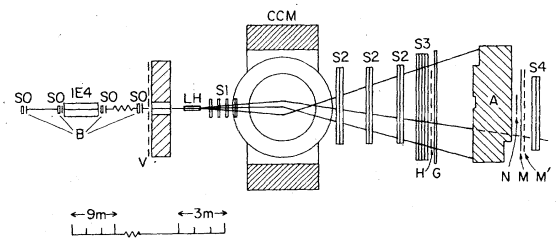

FIG. 4. Plan view of spectrometer. $S0$ and $S1$ are multiwire proportional chambers; $S2$, $S3$, and $S4$ are multiwire spark chambers; B, G, H, M, M', N, and V are counter hodoscopes; 1E4 and CCM are magnets; A is an absorber.

of muons entering the 120-cm liquid-hydrogen target (LH). If a muon interacted in the target, the products of that reaction were measured by a set of 1-m-square multiwire proportional chambers with 1.25-mm wire spacing ($S1$). Particles scattered in the forward direction were bent by the field of the large-aperture Chicago Cyclotron Magnet (CCM). Sets of spark chambers, $S2$ (2×4 m, 1.25-mm wire spacing), $S3$ (2×6 meter, 1.25-mm wire spacing), and $S4$ (2×4 m, 1.25-mm wire spacing) measured the trajectories of the particles after they were bent by the CCM. The tracks found in chambers $S1$–4 provided the information needed to calculate the vector momentum of products of the muon interaction.

The magnetic field of the CCM was cylindrically symmetric to better than 1%; this symmetry meant that the $S1$ and $S2$-$S3$ components of a particle trajectory had the same impact parameter to the magnet center. The resolution of the wire chamber system was such that the $S1$ to $S2$-$S3$ track linking had a resolution of 2 mm.

A 2–3-m steel absorber (A) absorbed the hadrons produced in the interaction. Muons penetrated this shield, caused triggers and were identified by spark chambers $S4$. Pion punchthrough was less than one percent.

Incident muons were bent through an angle of 28.4 mrad by the dipoles $1E4$. This magnet system and the beam chambers $S0$ measured the incident muon momentum to a resolution of 0.2%. The field integral in the spectrometer magnet CCM was 75 kG m or equivalently 2.25-GeV/c

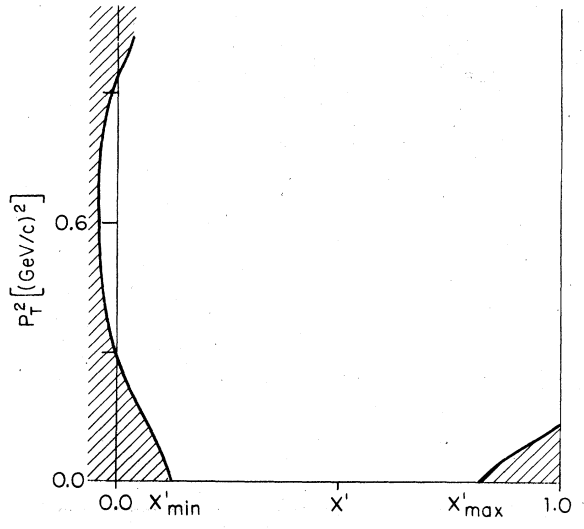

FIG. 5. Region of useful positive-hadron acceptance in x', p_T^2 phase space for event with $\nu = 100$ GeV, $Q^2 = 0.5$ (GeV/c)^2. Shaded regions have zero acceptance.

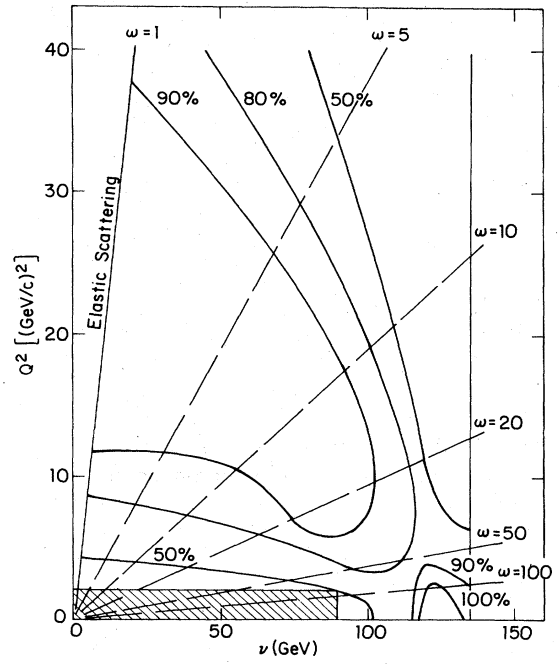

FIG. 6. Muon acceptance for the first-run data. The shaded area has no useful acceptance. The second-run data have improved acceptance in the shaded area.

transverse momentum. In conjunction with the track chamber modules $S1$–$S3$ the CCM was able to measure the momentum of 100-GeV particles to 1%.

One feature of the high transverse momentum of the CCM was that there was an approximate 8-GeV/c lower longitudinal-momentum cutoff for final-state particles. This meant that the lowest hadronic x' observable in an event was a strong function of ν (or s). In practice we observed particles with $x' > 0.08$ at $\nu > 100$ GeV with a proportional rise in the x' bound as ν decreased.

The spark-chamber module $S3$ was deadened in a circular region of 20 cm diameter about the beam. High-x' positive hadrons in low-Q^2, high-ν events would typically be lost in this region. This reduced the statistical accuracy of the high-x' positive-hadron data in some Q^2-ν regions. Figure 5 shows the region of x'-p_T^2 space where we had useful hadron acceptance for an event with $\nu = 100$ GeV, $Q^2 = 0.5$ (GeV/c)^2. Figure 6 shows the muon acceptance as a function of Q^2 and ν.

The experiment was designed so that the on-line data tape or any portion of it contained all information necessary to produce cross sections. Dead times, for example, were not calculated from separate data or runs. Some informative parameters describing the running are: beam

rate, 7.5×10^5/pulse; target densities, 8.4 g/cm^2 H_2, 20.1 g/cm^2 D_2; trigger rate $(6-10)\times10^{-6}$/ incident muon; total triggers, 7×10^5; integrated flux 3.7×10^{10} muons on H_2, 2.5×10^{10} muons on D_2. The data reported here were obtained in two separate runs: the first with hydrogen and deuterium targets and 147-GeV muons, the second with hydrogen only and 147-GeV muons.

V. DATA ANALYSIS

The first stage of the data analysis was the reconstruction of the muon scattering events from the raw data. We proceeded next to infer the final results, mostly structure functions, from these events without explicitly producing the muon inclusive cross section. Since structure functions are quantities measured per interaction rather than per incident particle, this was straightforward.

The sample of muon scatterings used for the hadron analysis was essentially that used to measure the muon inclusive scattering cross section. The latter analysis has already been cited. We have concentrated in this paper on the hadron analysis and will not discuss the details of the muon analysis.

A. Reconstruction of events

Three levels of data reduction were used to refine the raw data into kinematic events. The primary tapes were written by the Σ-3 computer during the run. The secondary tapes had wire-chamber information converted into true physical positions based on careful apparatus alignment studies. These tapes were the input to the track-finding programs. The tertiary tapes had counter and scaler information, the tracks found for each event, and kinematic quantities calculated for the particles found among the tracks.

Track finding was done independently in chamber modules *S*0, *S*1, *S*2-*S*3, and *S*4. Details of these programs will be found in the theses of Pordes (Harvard) and Kirkbride (Oxford). The most crucial module was *S*2-*S*3 as a particle had to be found here to be observed. The *S*2-*S*3 track-finding efficiency was 98% for most of the live region, but the efficiency dropped to 60% in the regions near the beam, mainly due to confusion caused by stale sparks. We studied these effects by searching for artificial tracks added to real data.

The track-finding in *S*2-*S*3 served as a basis with which to measure the trackfinding in the *S*1 (upstream) and *S*4 (muon) modules. Studies of good scattered muon events indicated that the *S*4 module had greater than 90% track-finding efficiency everywhere, while the chance of finding at least an x or y projection of a true track in the *S*1 module was between 90% and 95% depending on the data set.

The particular criteria to find a muon event were that: a track be found in *S*2-*S*3 such that elements of the counter hodoscopes G, H, M, M' that it struck were on; the tracks found in *S*2-*S*3 link to an x or y track in module *S*1; the *S*1 track(s) intersect the beam track in a physically possible location. Less than one percent of the muon events were consistent with having two or more muons; these were excluded from the analysis.

The interaction point for the event was determined initially by the intersection of the incident beam track (we used only those 70% of events where the beam system unambiguously reconstructed the incident particle) and the x, y track(s) belonging to the muon. Other tracks in *S*1 that linked to downstream *S*2-*S*3 tracks and were consistent with the muon only vertex were added to the χ^2 procedure that fit the vertex. The z position resolution of the vertex was thus dependent on the scattering angle or on Q^2; the transverse position resolution was mainly determined by the beam track. Events with $Q^2\geq0.3\,(\mathrm{GeV}/c)^2$ coming from the target and its vessel (94% liquid hydrogen by weight) were clearly distinguished from those of the upstream target vacuum wall (2 m upstream of the target center) and from the downstream proportional chambers *S*1. The events used in the analysis were those within 1.125 meters of the center of the 1.2-m-long target. We made no empty-target subtraction. Since we are presenting results per interaction, the small fraction of events that interacted in material other than liquid hydrogen or deuterium gives a negligible bias.

Hadron candidates associated with the muons were sorted into four classes for analysis purposes as well as being segregated by charge sign. All candidates were tracks in *S*2-*S*3 that had appropriate counter signatures in hodoscopes G and H (the counters were $\geq$99% efficient) and that linked to one or more x or y tracks in *S*1. Class 1 tracks had at least one linked upstream track passing close to the vertex at its z position. The actual distance for success was about 1mm, but this varied depending on the z resolution of the vertex. Class 1 status also required that the y projection of the candidate *S*2-*S*3 track pass within 60 mm of the vertex. A slight correction was made for the y plane focussing due to bending in the magnet. This downstream y linking helped to prevent halo tracks from contaminating the hadron sample. Another requirement used to reduce halo contamination was that class 1 candidates linking to muon

TABLE IV. Class breakdown of hadron candidates for hydrogen data.

Class	No. of hadron candidates with $p_T^2 \leq 3.0$ (GeV/c)^2 Negatives	Positives
1	5035	5005
2	239	332
3	253	586
4	228	627

tracks in module $S4$ were reduced to class 3 status unless they linked to the vertex with x and y tracks in $S1$. We initially removed all class 1 tracks that linked in $S4$, but we found from looking at ρ^0 meson events that this cut was removing real hadrons. Class 2 candidates were like class 1, but the downstream vertex y linking failed. Class 3 candidates were like class 1, but with no upstream linking. Class 4 candidates were the remainder.

Table IV shows the breakdown of hadron candidates for the hydrogen data. Only 13% of all the negative candidates did not achieve class 1. The 25% fraction of the positive candidates below class 1 is larger than the negative ratio because of the intrusion of halo muons.

From a comparison of the rate of x and y upstream vertex linking to that for x only or y only upstream linking, we get a 96% efficiency for a real hadron whose track in $S2$-$S3$ is found to be class 1.

On the other hand, when we calculate the x' and p_T^2 of class 2 through class 4 candidates (this only requires knowledge of the vertex and the $S2$-$S3$ track), we find that many of these events distribute themselves in a x', p_T^2 space in a manner similar to the class 1 candidates. Using events in the most highly populated low-x', low-p_T^2 regions, we get a worst case analysis efficiency of 88% assuming that all such class 2 through class 4 candidates are real hadrons. We used only class 1 hadrons in the analysis and assigned an efficiency to them of (92 ± 4)%. The same conclusions were reached for the deuterium data.

Despite the precautions taken, muon halo did leak into the positive hadron sample. We made some additional cuts besides those described. We eliminated all hadrons having energy greater than the incident muon energy loss plus 4 GeV. Examination of the data showed that eliminating hadrons having $p_T^2 > 3.0$ (GeV/c)^2 had negligible effect on the real data, but cut out many halo hadrons.

A worst case estimate of the contamination of the positive-hadron sample was made as follows: 20% of the class 3 and 4 positive hadrons were expressed as a fraction of the class 1 positive hadrons (muon linking efficiency is greater than 90%). This fraction is taken as the systematic error on the muon contamination and is 6% for $x' \geq 0.3$, 3% for $x' \leq 0.3$ for hydrogen. The corresponding numbers are 8% and 4% for deuterium. We estimate that there was a loss of real positive events due to muon linking that was less than or equal to these gains from muon contamination.

We made no corrections to the data for apparatus resolution. Preliminary calculations showed such effects to be negligible given the statistical errors, data bin sizes, and the high spatial resolution of the spectrometer. The bulk of the muon events also occur in the low-Q^2, high-ν region where the measurement of the virtual photon's three-momentum is least dependent on the measurement of the scattered muon. The angular resolution in the measurement of a final-state particle track upstream of the CCM was less than 1 mrad. In the case of ρ^0 mesons the width of the $\pi^+\pi^-$ mass distribution was dominated by the ρ^0 width.[27]

B. Direct corrections to events

In forming the final results, the observed number of hadrons was directly weighted by four factors. These were the hadron identification efficiency described above, the $S2$-$S3$ track-finding efficiency which was position dependent, the muon and hadron acceptance and the efficiency for the hadron to pass out of the target unscattered. The muon acceptance was taken from the parallel muon inclusive analysis and is shown in Fig. 6. The hadron acceptance was an azimuthal average at fixed x' and p_T^2 about the virtual-photon direction. The measurement of the ϕ distribution of the hadrons, discussed below, showed the azimuthal average to be a reasonable procedure.

All events were weighted by an average probability that they would not rescatter inelastically in the target. Secondaries from such interactions would typically fall below the 8-GeV/c momentum cutoff of the magnet or at worst contribute to a part of the cross section much larger than that from which they originated. The average interaction rate was 5% for hydrogen and 11% for deuterium.

C. Cuts on events

The $Q^2 \geq 0.3$ (GeV/c)^2 cut on events which we used to define the target also conveniently eliminated elastic muon-electron scatters. We were able to identify ρ^0 mesons by plotting the total energies of hadron pairs as a fraction of the en-

ergy lost by the incident muon. A clear peak in this distribution of about three times background was observed between hadron pair energy fractions of 0.96 and 1.04. A mass plot, assuming final-state pions, of these elastic pairs showed that above $Q^2 = 0.3$ (GeV/c)^2, 70% of these pairs were ρ^0 mesons, and the rest were piled up at the lowest mass possible indicating they were likely electron-positron pairs. These events were less than one percent of the muon scatters and were removed from the data sample.

D. Radiative corrections

To interpret the results of muon or electron scattering experiments, one must assess the effects of radiative corrections. These come about because diagrams similar to Fig. 1 in which the incident or scattered muon emits a real photon contribute significantly to the observed muon scattering. The important effects for this hadron analysis were: (a) Substantial numbers of events at low Q^2 [$Q^2 \leq 2$ (GeV/c)^2] and high ν ($\nu \geq 80$ GeV) were not hadronic events, but rather were muon bremsstrahlung events with a fairly large elastic momentum transfer to the target nucleon; (b) the loss of energy to radiative photons caused us to misestimate the direction of the virtual photon and overestimate its energy.

We made a correction to the number of observed muon scatters to remove the purely radiative events. For the hydrogen data in the bin $0.5 < Q^2 < 3.0$ (GeV/c)^2; $s > 100$ GeV^2, we estimated 17% of the events were radiative only. The average corrections to the other hydrogen data bins were 5% or less. The corresponding deuterium-data corrections were half those of hydrogen. These estimates came from the muon inclusive analysis and were based on the method of Mo and Tsai.[28]

No other radiative corrections were made to the data. However, following a paper by Tsai[29] we can estimate the magnitude of the error in the apparent transverse momentum of hadrons because of the error in the apparent virtual-photon direction. Tsai finds the following formula for the average angle between true and apparent virtual-photon directions for radiative energy loss Δ:

$$\theta_{qq'} = \frac{(E_\mu E'_\mu)^{1/2}}{(\nu^2 + Q^2)} \Delta \sin\theta_\mu . \tag{27}$$

A hadron having $z\nu$ energy in the lab frame will have its transverse momentum in the muon scattering plane misestimated by an amount δP_T,

$$\delta p_T = z\nu\theta_{qq'} . \tag{28}$$

For most quantities of physical interest δP_T will be added in quadrature to existing transverse-momentum components so that,

$$\langle \delta p_T{}^2 \rangle = z^2\nu^2 \frac{E_\mu E'_\mu}{(\nu^2 + Q^2)^2} \langle \Delta^2 \rangle \sin^2\theta_\mu . \tag{29}$$

To a good approximation the distribution of energy losses follows a $1/\Delta$ distribution, but in the case of observing a hadron of apparent energy fraction z the energy loss cannot exceed $(1 - z)$. Therefore,

$$\langle \Delta^2 \rangle \cong \int_0^{\nu(1-z)} \Delta^2 \frac{2\alpha}{\pi} \left(\ln \frac{Q^2}{m_\mu{}^2} - 1 \right) \frac{d\Delta}{\Delta} \left(1 - \frac{\Delta}{(E_\mu E'_\mu)^{1/2}} \right)$$

$$\cong \frac{\alpha}{\pi} \left[\ln \left(\frac{Q^2}{m_\mu{}^2} \right) - 1 \right] \nu^2 (1 - z)^2 , \tag{30}$$

$$\langle \delta p_T{}^2 \rangle \cong \frac{\alpha}{\pi} \left[\ln \left(\frac{Q^2}{m_\mu{}^2} \right) - 1 \right] (1 - z^2) z^2 Q^2 . \tag{31}$$

For example, with $z = \frac{1}{2}$ and $Q^2 = 12$ (GeV/c)^2,

$\langle \delta p_T{}^2 \rangle = 0.01$ (GeV/c)^2.

E. Calculation of results

The structure function $(E/\sigma)(d^3\sigma/dp^3)$, which is typical of the results in this paper, is estimated by the formula:

$$\frac{E}{\sigma} \frac{d^3\sigma}{dp^3}(\overline{x'}, \overline{p_T{}^2}, \overline{Q^2}, \overline{\nu})$$

$$= \frac{1}{\pi \Delta x' \Delta p_T{}^2} \frac{\sum_{\Delta Q^2, \Delta s, \Delta x', \delta p_T{}^2} \frac{E^*}{(P_{\max}{}^2 - p_T{}^2)^{1/2}} \frac{1}{\epsilon_\mu} \frac{1}{\epsilon_h}}{\sum_{\Delta Q^2, \Delta s} \frac{1}{\epsilon_\mu} [1 - \delta R(Q^2, s)]} , \tag{32}$$

where ΔQ^2, Δs, $\Delta x'$, $\Delta p_T{}^2$ define the muon and hadron kinematic bin for which the estimate is made; ϵ_h is the complete hadron acceptance and efficiency; ϵ_μ is the muon acceptance; $\delta R(Q^2, s)$ is the probability that the muon bremsstrahlungs only; the top summation is over all hadrons in ΔQ^2, Δs, $\Delta x'$, and $\Delta p_T{}^2$; the bottom summation is over all muons in ΔQ^2 and Δs for which there is nonzero hadron acceptance in $\Delta x'$ and $\Delta p_T{}^2$.

To estimate the charge ratio N^+/N^-, we divided the weighted number of positive hadrons in one bin by the weighted number of negative hadrons in the corresponding bin. However, because of the deadener in the 6-m chambers, (S3), the acceptance was very different for high-momentum negative and positive hadrons. To symmetrize the acceptance, a virtual deadener was given the same radius as the real deadener and was symmetrically positioned, horizontally, about the virtual photon's projected position in the 6-m chamber. Only hadrons which missed both dead-

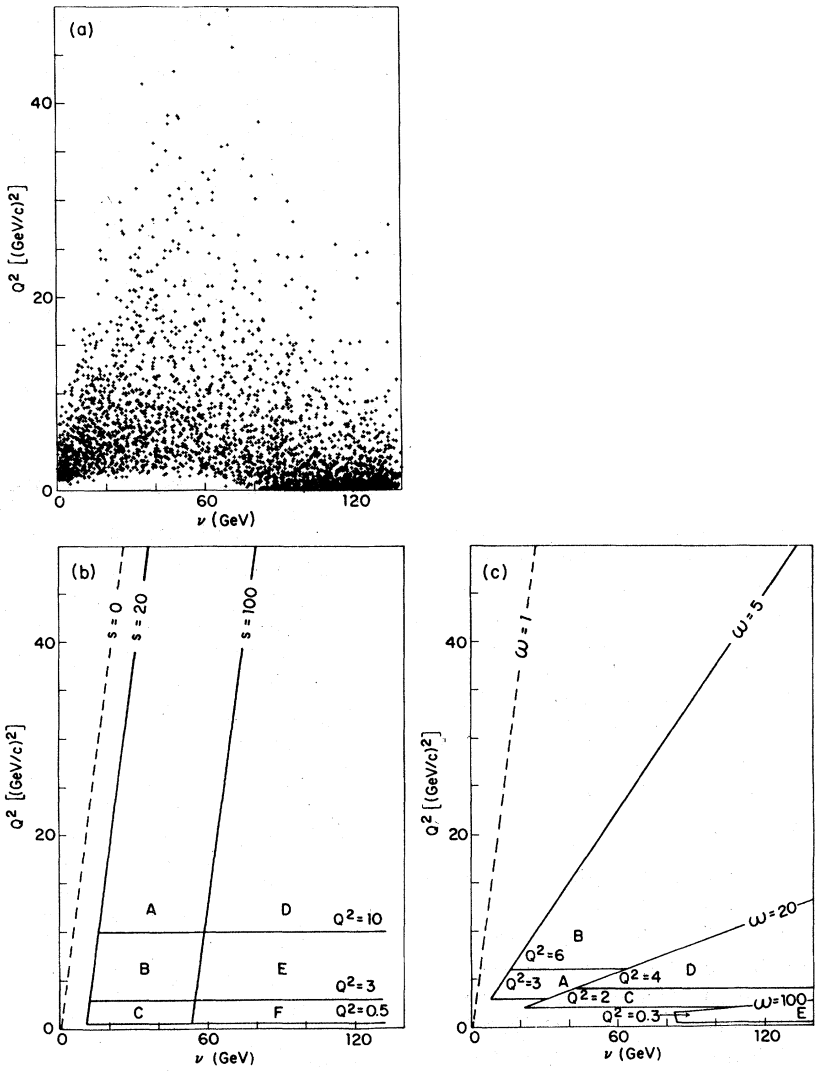

FIG. 7. (a) Q^2-ν scatter plot for hydrogen events from first-run data. (b) Q^2-s bins used; (c) Q^2-ω bins used. s is given in units of GeV^2.

eners were used in calculating the charge ratios.

We used the following formula to obtain neutron-target results from proton and deutron data:

$$F_n(x') = \frac{\sigma_d}{\sigma_n} F_d(x') - \frac{\sigma_p}{\sigma_n} F_p(x') . \tag{33}$$

This formula is stated for longitudinal structure function, but applies to any structure functions. We are in effect assuming that deuterium is a mixture of neutrons and protons with negligible interactions between neutron and proton. These subtractions are, naturally, very sensitive to systematic differences between photon and deuteron data. The ratios σ_d/σ_n and σ_p/σ_n were taken from precise measurements at low energy.[30]

A different approach to the hadron acceptance was used to obtain the azimuthal distribution of hadrons about the virtual photon. The quantity $d\sigma/d\phi$ was determined as a function of Q^2, ϵ, and x'. We divided the azimuth into many small bins. The cross section for each bin was estimated (aside from the overall normalization which was arbitrary) as

$$\frac{d\sigma}{d\phi_{\Delta\phi}} \propto \frac{\sum_{\Delta\phi, \Delta x', \Delta Q^2, \Delta\epsilon} \frac{1}{\epsilon_\mu}}{\sum_{\Delta x', \Delta Q^2, \Delta\epsilon} \frac{1}{\epsilon_\mu}} , \tag{34}$$

where $\Delta\phi$, $\Delta x'$, ΔQ^2, $\Delta\epsilon$ define the bin for which

the estimate is made; the top summation is over all muon-hadron combinations in $\Delta\phi$, $\Delta x'$, ΔQ^2, and $\Delta\epsilon$; the bottom summation is over all muon-hadron combinations in $\Delta x'$, ΔQ^2, $\Delta\epsilon$ that would have unit acceptance in $\Delta\phi$. The number of hadrons in each $\Delta\phi$ bin in effect is normalized by the number of muons which had perfect acceptance for any hadron produced in $\Delta\phi$.

F. Binning of the data

The data covered a wide range of Q^2 and ν. However, the overall statistics did not permit fine binning. An important aspect of the data is the variation of the hadronic properties with Q^2 and s or Q^2 and ω. A Q^2-ν scatter plot of the first-run hydrogen data is shown in Fig. 7. We used for the most part the Q^2-s bins of Fig. 7(b) or the Q^2-ω bins of Fig. 7(c) in determining the hadronic dependence of the muon kinematics. The bins used do not cover the full range of Q^2 and ν available to us. The hadron acceptance in the regions excluded was very poor and little could be learned by their inclusion. The total numbers of events used in the analysis were 8.5×10^3 for hydrogen and 10.3×10^3 for deuterium.

VI. RESULTS

Hadron leptoproduction data are more complex than the corresponding muon inclusive data; there is no widely used formulation to present the data that shows the full complexity naturally and has a sound theoretical footing. Our approach in this section is to describe the data and compare it to previous measurements. We then discuss the data in terms of the theoretical expectations previously outlined.

A. General description of the data

The longitudinal hadronic structure functions for the proton, the deuteron, and the neutron, $F^{\pm}(x')$ are shown in Figs. 8 and 9. The data are displayed for various Q^2 and ω ranges in the first figure and for Q^2 and s ranges in the second. Because of inadequate statistics, the neutron function is not shown for some regions. The dashed line is $0.35\exp(-3.25x')$ and is a guide for intercomparisons. This line is a good representation of the negative-hadron structure function of a lower-energy electron-proton experiment.[31] Tables V and VI are listings of these data; Table VII gives values of $(1/\sigma)d\sigma/dz$ for the same Q^2 and ω ranges as Table V.

The major feature of the data are as follows:

1. Variations of the structure functions with the muon kinematic variables are evident but are not large. The data for proton, neutron, and deuteron are similar to each other.

2. For $x'\geq0.2$ the positive-charge structure function is equal to or larger than the negative one. This difference appears to increase with x' for fixed Q^2 and s or ω and also to increase with Q^2 for decreasing ω at fixed x'. Overall the positive and negative structure functions appear to scale on the average (i.e., $F^+ + F^-$ is constant as a function of Q^2) as indicated by how the guideline typically lies between F^+ and F^-.

3. For $x'\leq0.2$ the positive and negative structure functions are equal and they scale with muon kinematic variables. The Q^2 and ω variations of the struction functions are clearly illustrated in Fig. 10. At $\langle x'\rangle=0.44$ the positive and negative structure functions approximately average to a constant. The increase with ω of the positive structure function at $\langle x'\rangle=0.44$ and the corresponding decrease of the negative function at $\langle x'\rangle=0.44$, while the structure functions at $\langle x'\rangle=0.14$ remain constant, indicate that the former function flattens and the latter steepens with decreasing ω.

The features of these data are consistent with previous measurements of the multiplicity of hadrons in electroproduction.[32] The multiplicity was found to be independent of Q^2 and to increase approximately as the natural logarithm of the center-of-mass energy s. For hadrons in the center-of-mass frame whose energy is larger than their mass and/or transverse momentum, $F(x')$ apart from a factor of π is just the momentum-weighted multiplicity distribution, $F(x')\simeq(x'/\pi\sigma)(d\sigma/dx)$. The data clearly show that most hadrons occur at low x'. The constancy of multiplicity would thus force $F(x')$ at low x' to be constant as well if we ignore some extreme possibilities. Again, since charge is conserved and multiplicity grows with energy, the number of negative and positive charged particles occurring at low x' must tend towards equality forcing $F^+(x')=F^-(x')$.

To get a better intuitive idea of the characteristics of muoproduced hadrons, we can use the approximate form for $F(x')$ [Table III (the same discussion may be conducted using $F(z)$)]. We have after transposition:

$$\frac{1}{\sigma}\frac{d\sigma}{dx'}\cong\frac{\pi}{x'}F(x')\,. \tag{35}$$

The value of x', x_1', for which

$$\int_{x_1'}^{1}dx'\left(\frac{1}{\sigma}\frac{dx^+}{dx'}+\frac{1}{\sigma}\frac{d\sigma^-}{dx'}\right)=1 \tag{36}$$

is the value of x' above which there is on the average one charged particle in a virtual-photon-

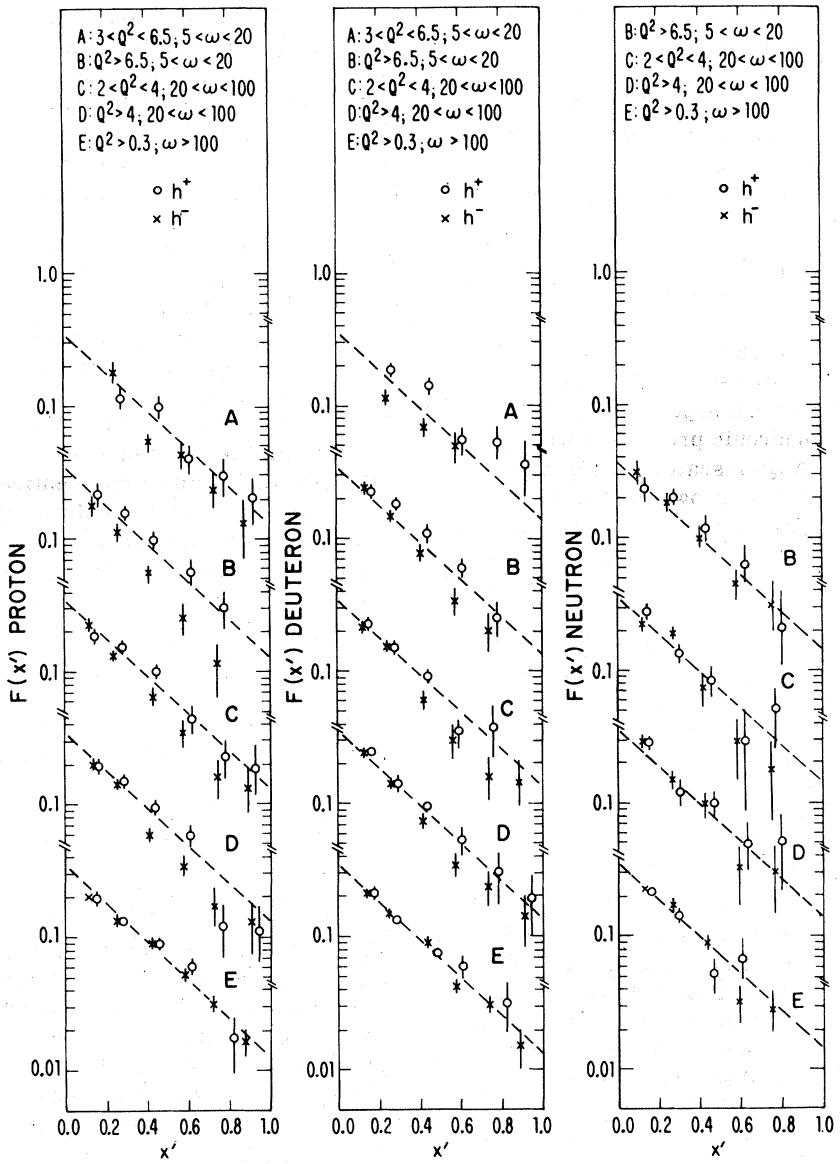

FIG. 8. Proton, deuteron and neutron structure functions for different ranges of Q^2 and ω. The dashed line is 0.35 $\exp(-3.25x')$. The Q^2 ranges are in units of $(\mathrm{GeV}/c)^2$.

nucleon interaction. Evaluating this integral from our data leads to $x_1' = 0.16 \pm 0.02$ where the error is an overestimate but adequate for this purpose. If we assume there are as many neutral particles as there are particles of each charge, x_1' would be $x_1' \cong 0.22 \pm 0.02$. The value of x' above which there are two particles, charged or neutral, is similarly $x_2' \cong 0.13 \pm 0.03$.

Using this rough analysis we can further determine the average x' of particles in the region $x' > x_1'$. This will be approximately the x' of the leading particle of produced hadrons. We have

$$\langle x' \rangle = \frac{\int_{x_1'}^{1} \frac{x'}{\sigma} \frac{d\sigma}{dx'} dx'}{\int_{x_1'}^{1} \frac{1}{\sigma} \frac{d\sigma}{dx'} dx'} = 0.44 \pm 0.06 . \tag{37}$$

The leading particle thus has about half the total virtual-photon energy. This is a valid conclusion in both the center-of-mass and lab systems.

It is interesting to know in the same approximate sense used above how much of the virtual photon's

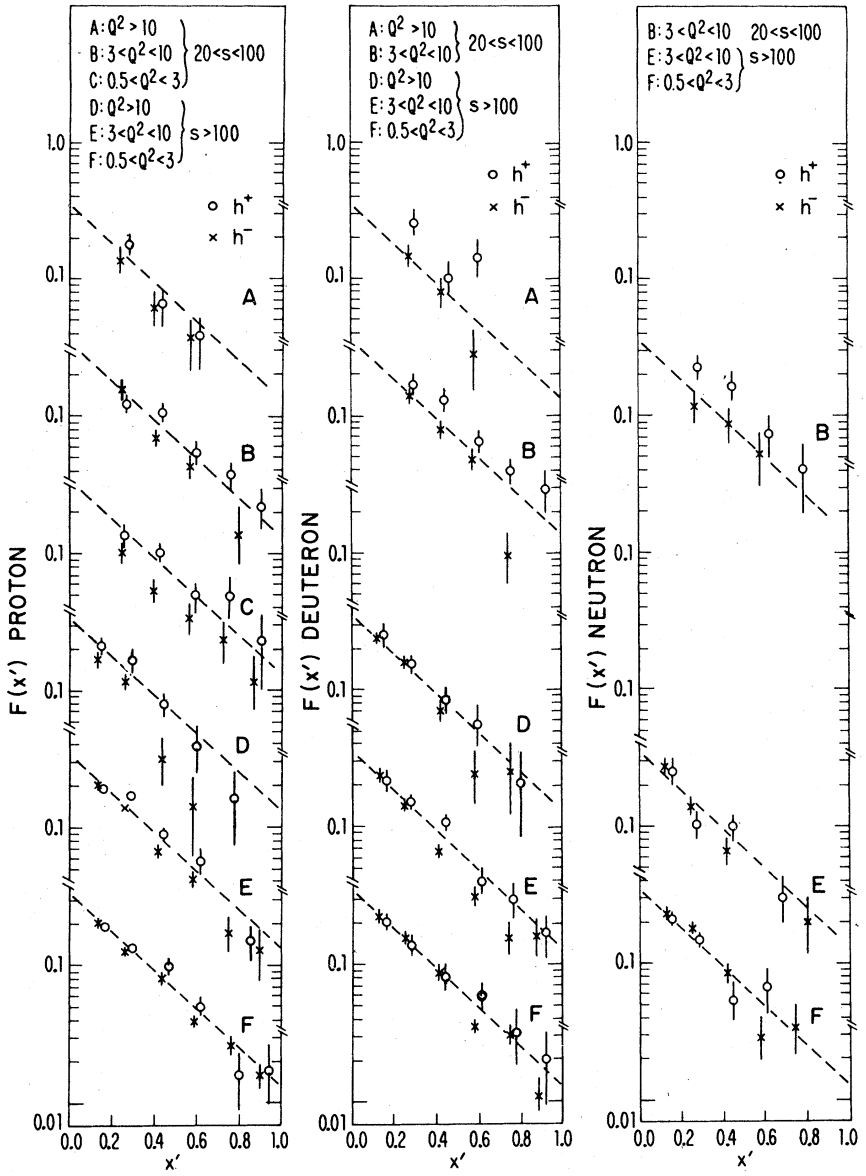

FIG. 9. Proton, deuteron, and neutron structure functions for different ranges of Q^2 and s. The dashed line is $0.35\exp(-3.25x')$. The Q^2 ranges are in units of $(\mathrm{GeV}/c)^2$ and the s ranges are in units of GeV^2.

energy ends up in charged hadrons. This fraction, for each charge is given by $I^{\pm}$:

$$I^{\pm} = \pi \int_0^1 F^{\pm}(x')dx'$$

$$= \int_0^1 dx' \int_0^{p_{T\max}^2} dp_T^2 \frac{1}{\sigma} \frac{E^*}{(p^* - p_T^2)^{1/2}} \frac{d^2\sigma}{dx'\,dp_T^2}. \quad (38)$$

Using the hydrogen data in Fig. 8 and assigning the value of 0.23 ± 0.1 to the structure function in the region $0.0 < x' < 0.08$, we find $I^+ + I^- = 0.59 \pm 0.05$. This is in accord with most of the photon's initial energy ending up as pions through isospin conserving processes.

The structure function $(E/\sigma)\,(d^3\sigma/dp^3)$ is shown in Fig. 11 for hydrogen and deuterium. The data used are for $Q^2 > 0.3$ $(\mathrm{GeV}/c)^2$, $s > 100$ GeV^2, and $\omega > 40$. We fit the data with the form

$$\frac{E}{\sigma}\frac{d^3\sigma}{dp^3} = A\left[\exp\left(\frac{-2bp_T^2}{1+(1+p_T^2/\mathfrak{M}^2)^{1/2}}\right)\right]. \quad (39)$$

TABLE V. Structure function $F(x')$ for proton, deuteron, and neutron targets in Q^2-ω bins. Statistical errors only. There is an overall systematic error of ±4%. Positive-hadron data for $x' > 0.3$ have additional errors described in the text.

Target and muon kinematics	Charge	x' 0.08 – 0.20	0.2 – 0.36	0.36 – 0.52	0.52 – 0.68	0.68 – 0.84	0.84 – 1.0
Proton							
$3<Q^2<6$ (GeV/c)^2, $5<\omega<20$	−		0.172 ± 0.034	0.059 ± 0.011	0.040 ± 0.011	0.022 ± 0.007	0.014 ± 0.009
	+		0.113 ± 0.017	0.098 ± 0.016	0.042 ± 0.011	0.028 ± 0.01	0.021 ± 0.009
$Q^2>6$ (GeV/c)^2, $5<\omega<20$	−	0.171 ± 0.023	0.110 ± 0.010	0.055 ± 0.009	0.026 ± 0.009	0.011 ± 0.005	
	+	0.231 ± 0.028	0.166 ± 0.013	0.106 ± 0.012	0.059 ± 0.011	0.031 ± 0.008	
$2<Q^2<4$ (GeV/c)^2, $20<\omega<100$	−	0.219 ± 0.016	0.126 ± 0.084	0.063 ± 0.007	0.035 ± 0.006	0.017 ± 0.005	0.013 ± 0.004
	+	0.186 ± 0.012	0.155 ± 0.011	0.103 ± 0.011	0.044 ± 0.008	0.025 ± 0.007	0.018 ± 0.001
$Q^2>4$ (GeV/c)^2, $20<\omega<100$	−	0.190 ± 0.017	0.138 ± 0.011	0.054 ± 0.008	0.034 ± 0.007	0.017 ± 0.007	0.012 ± 0.006
	+	0.208 ± 0.015	0.158 ± 0.013	0.097 ± 0.013	0.059 ± 0.013	0.011 ± 0.006	0.011 ± 0.006
$Q^2>0.3$ (GeV/c)^2, $\omega>100$	−	0.197 ± 0.007	0.128 ± 0.006	0.091 ± 0.006	0.053 ± 0.005	0.031 ± 0.005	0.016 ± 0.004
	+	0.204 ± 0.007	0.139 ± 0.006	0.090 ± 0.008	0.057 ± 0.012	0.019 ± 0.011	
Deuteron							
$3<Q^2<6$ (GeV/c)^2, $5<\omega<20$	−		0.114 ± 0.016	0.063 ± 0.012	0.046 ± 0.013		
	+		0.187 ± 0.025	0.141 ± 0.023	0.053 ± 0.014	0.056 ± 0.016	0.037 ± 0.017
$Q^2>6$ (GeV/c)^2, $5<\omega<20$	−	0.234 ± 0.028	0.142 ± 0.012	0.074 ± 0.010	0.034 ± 0.007	0.020 ± 0.008	
	+	0.230 ± 0.024	0.182 ± 0.014	0.110 ± 0.014	0.060 ± 0.011	0.026 ± 0.008	0.013 ± 0.006
$2<Q^2<4$ (GeV/c)^2, $20<\omega<100$	−	0.214 ± 0.014	0.152 ± 0.011	0.066 ± 0.008	0.031 ± 0.006	0.017 ± 0.005	0.014 ± 0.006
	+	0.229 ± 0.013	0.143 ± 0.010	0.092 ± 0.011	0.036 ± 0.009	0.037 ± 0.012	
$Q^2>4$ (GeV/c)^2, $20<\omega<100$	−	0.234 ± 0.019	0.139 ± 0.011	0.073 ± 0.009	0.032 ± 0.007	0.023 ± 0.007	0.014 ± 0.006
	+	0.237 ± 0.015	0.137 ± 0.012	0.096 ± 0.012	0.053 ± 0.010	0.030 ± 0.013	0.020 ± 0.009
$Q^2>0.3$ (GeV/c)^2, $\omega>100$	−	0.205 ± 0.005	0.145 ± 0.005	0.088 ± 0.005	0.042 ± 0.004	0.030 ± 0.004	0.014 ± 0.003
	+	0.205 ± 0.005	0.138 ± 0.005	0.076 ± 0.005	0.061 ± 0.011	0.019 ± 0.11	
Neutron							
$Q^2>6$ (GeV/c)^2, $5<\omega<20$	−	0.303 ± 0.06	0.177 ± 0.025	0.095 ± 0.022	0.043 ± 0.01	0.030 ± 0.017	
	+	0.228 ± 0.05	0.199 ± 0.030	0.114 ± 0.030	0.061 ± 0.024	0.020 ± 0.018	
$2<Q^2<4$ (GeV/c)^2, $20<\omega<100$	−	0.209 ± 0.030	0.178 ± 0.022	0.069 ± 0.018	0.027 ± 0.013	0.017 ± 0.010	
	+	0.273 ± 0.028	0.131 ± 0.022	0.081 ± 0.024	0.028 ± 0.020	0.049 ± 0.024	
$Q^2>4$ (GeV/c)^2, $20<\omega<100$	−	0.279 ± 0.04	0.140 ± 0.024	0.092 ± 0.020	0.030 ± 0.014	0.029 ± 0.015	
	+	0.267 ± 0.03	0.115 ± 0.026	0.095 ± 0.025	0.047 ± 0.021	0.049 ± 0.028	
$Q^2>0.3$ (GeV/c)^2, $\omega>100$	−	0.213 ± 0.012	0.162 ± 0.011	0.085 ± 0.011	0.031 ± 0.009	0.029 ± 0.009	0.012 ± 0.007
	+	0.206 ± 0.012	0.137 ± 0.011	0.062 ± 0.013	0.065 ± 0.022	0.019 ± 0.024	

TABLE VI. Structure function $F(x')$ for proton, deuteron, and neutron targets in Q^2-s bins. Statistical errors only. There is an additional systematic error of ±4%. Positive-hadron data for $x' > 0.3$ have additional errors described in the text.

Target and muon kinematics	Charge	x' 0.08 – 0.20	0.20 – 0.36	0.36 – 0.52	0.52 – 0.68	0.68 – 0.84	0.84 – 1.0
Proton							
$0.5 < Q^2 < 3.0$ (GeV/c)^2, $20 < s < 100$ (GeV)^2	−		0.097 ± 0.015	0.052 ± 0.010	0.038 ± 0.010	0.023 ± 0.008	
	+		0.130 ± 0.019	0.106 ± 0.016	0.051 ± 0.012	0.056 ± 0.017	0.023 ± 0.01
$3.0 < Q^2 < 10.0$ (GeV/c)^2, $20 < s < 100$ (GeV)^2	−		0.146 ± 0.018	0.064 ± 0.009	0.042 ± 0.009	0.016 ± 0.005	
	+		0.119 ± 0.012	0.100 ± 0.011	0.052 ± 0.009	0.035 ± 0.009	0.022 ± 0.007
$Q^2 > 10.0$ (GeV/c)^2, $20 < s < 100$ (GeV)^2	−		0.130 ± 0.025	0.065 ± 0.018	0.036 ± 0.017		
	+		0.184 ± 0.029	0.046 ± 0.014	0.025 ± 0.013		
$0.5 < Q^2 < 3.0$ (GeV/c)^2, $s > 100$ (GeV)^2	−	0.197 ± 0.007	0.127 ± 0.006	0.081 ± 0.006	0.040 ± 0.004	0.025 ± 0.004	0.016 ± 0.004
	+	0.200 ± 0.007	0.139 ± 0.006	0.097 ± 0.008	0.055 ± 0.009	0.019 ± 0.008	0.017 ± 0.010
$3.0 < Q^2 < 10.0$ (GeV/c)^2, $s > 100$ (GeV)^2	−	0.198 ± 0.013	0.137 ± 0.009	0.064 ± 0.007	0.038 ± 0.006	0.018 ± 0.005	0.010 ± 0.004
	+	0.191 ± 0.011	0.176 ± 0.010	0.094 ± 0.010	0.062 ± 0.010	0.017 ± 0.006	0.013 ± 0.006
$Q^2 > 10.0$ (GeV/c)^2, $s > 100$ (GeV)^2	−	0.160 ± 0.024	0.118 ± 0.017	0.034 ± 0.011	0.014 ± 0.008		
	+	0.226 ± 0.030	0.158 ± 0.020	0.077 ± 0.016	0.038 ± 0.013	0.015 ± 0.008	
Deuteron							
$3.0 < Q^2 < 10.0$ (GeV/c)^2, $20 < s < 100$ (GeV)^2	−		0.132 ± 0.013	0.074 ± 0.010	0.047 ± 0.010	0.011 ± 0.004	
	+		0.173 ± 0.016	0.134 ± 0.016	0.062 ± 0.011	0.041 ± 0.010	0.027 ± 0.011
$Q^2 > 10.0$ (GeV/c)^2, $20 < s < 100$ (GeV)^2	−		0.143 ± 0.027	0.078 ± 0.023	0.028 ± 0.014		
	+		0.262 ± 0.040	0.097 ± 0.024	0.134 ± 0.040		
$0.5 < Q^2 < 3.0$ (GeV/c)^2, $s > 100$ (GeV)^2	−	0.213 ± 0.007	0.153 ± 0.006	0.083 ± 0.006	0.035 ± 0.004	0.029 ± 0.005	0.011 ± 0.003
	+	0.205 ± 0.006	0.143 ± 0.006	0.075 ± 0.006	0.060 ± 0.012	0.034 ± 0.012	
$3.0 < Q^2 < 10.0$ (GeV/c)^2, $s > 100$ (GeV)^2	−	0.231 ± 0.014	0.136 ± 0.008	0.067 ± 0.007	0.030 ± 0.005	0.015 ± 0.004	0.017 ± 0.005
	+	0.222 ± 0.011	0.141 ± 0.009	0.097 ± 0.009	0.040 ± 0.007	0.030 ± 0.009	0.013 ± 0.006
$Q^2 > 10.0$ (GeV/c)^2, $s > 100$ (GeV)^2	−	0.229 ± 0.029	0.160 ± 0.019	0.068 ± 0.015	0.024 ± 0.010	0.024 ± 0.014	
	+	0.250 ± 0.027	0.158 ± 0.020	0.073 ± 0.015	0.058 ± 0.018	0.021 ± 0.013	0.016 ± 0.010
Neutron							
$3.0 < Q^2 < 10.0$ (GeV/c)^2, $20 < s < 100$ (GeV)^2	−		0.116 ± 0.033	0.084 ± 0.022	0.053 ± 0.023		
	+		0.232 ± 0.036	0.170 ± 0.037	0.071 ± 0.025	0.048 ± 0.073	
$0.5 < Q^2 < 3.0$ (GeV/c)^2, $s > 100$ (GeV)^2	−	0.229 ± 0.015	0.178 ± 0.013	0.084 ± 0.029	0.028 ± 0.008	0.033 ± 0.011	
	+	0.209 ± 0.014	0.146 ± 0.014	0.052 ± 0.015	0.066 ± 0.026		
$3.0 < Q^2 < 10.0$ (GeV/c)^2, $s > 100$ GeV^2	−	0.265 ± 0.032	0.135 ± 0.018	0.070 ± 0.016	0.020 ± 0.006		
	+	0.255 ± 0.025	0.104 ± 0.020	0.100 ± 0.022	0.030 ± 0.012		

TABLE VII. Structure function $(1/\sigma)d\sigma/dz$ for proton and deuteron targets in Q^2-ω bins. Statistical errors only. There is an overall systematic error of ±4%. Positive-hadron data for $x' > 0.3$ have additional systematic errors described in the text.

Target and muon kinematics	Charge	z: 0.08 – 0.20	0.2 – 0.36	0.36 – 0.52	0.52 – 0.68	0.68 – 0.84	0.84 – 1.0
Proton							
$3<Q^2<6$ (GeV/c)^2, $5<\omega<20$	−		2.02 ± 0.31	0.487 ± 0.083	0.192 ± 0.050	0.097 ± 0.028	
	+		1.55 ± 0.21	0.647 ± 0.010	0.251 ± 0.061	0.110 ± 0.038	
$Q^2>6$ (GeV/c)^2, $5<\omega<20$	−	3.85 ± 0.59	1.26 ± 0.11	0.431 ± 0.061	0.138 ± 0.040	0.044 ± 0.019	
	+	5.16 ± 0.60	1.88 ± 0.15	0.748 ± 0.087	0.304 ± 0.057	0.129 ± 0.033	
$2<Q^2<4$ (GeV/c)^2, $20<\omega<100$	−	5.56 ± 0.46	1.55 ± 0.10	0.455 ± 0.045	0.188 ± 0.034	0.069 ± 0.021	0.044 ± 0.015
	+	4.36 ± 0.30	1.86 ± 0.12	0.744 ± 0.078	0.285 ± 0.046	0.116 ± 0.031	0.059 ± 0.025
$Q^2>4$ (GeV/c)^2, $20<\omega<100$	−	4.44 ± 0.41	1.57 ± 0.13	0.424 ± 0.062	0.188 ± 0.040	0.069 ± 0.027	0.041 ± 0.020
	+	4.89 ± 0.37	1.94 ± 0.15	0.729 ± 0.092	0.313 ± 0.067	0.048 ± 0.025	0.039 ± 0.022
$Q^2>0.3$ (GeV/c)^2, $\omega>100$	−	4.74 ± 0.15	1.55 ± 0.06	0.666 ± 0.043	0.284 ± 0.027	0.132 ± 0.019	0.053 ± 0.012
	+	4.85 ± 0.16	1.64 ± 0.07	0.666 ± 0.056	0.303 ± 0.060	0.071 ± 0.041	
Deuteron							
$3<Q^2<6$ (GeV/c)^2, $5<\omega<20$	−		1.17 ± 0.16	0.481 ± 0.083	0.201 ± 0.056		
	+		2.01 ± 0.25	1.08 ± 0.16	0.322 ± 0.079	0.236 ± 0.066	0.135 ± 0.061
$Q^2>6$ (GeV/c)^2, $5<\omega<20$	−	4.77 ± 0.76	1.62 ± 0.12	0.597 ± 0.078	0.182 ± 0.040	0.078 ± 0.031	
	+	4.99 ± 0.55	2.12 ± 0.15	0.810 ± 0.093	0.339 ± 0.063	0.113 ± 0.033	
$2<Q^2<$ (GeV/c)^2, $20<\omega<100$	−	5.31 ± 0.37	1.76 ± 0.11	0.528 ± 0.061	0.167 ± 0.034	0.078 ± 0.023	0.044 ± 0.018
	+	5.65 ± 0.34	1.79 ± 0.12	0.682 ± 0.079	0.197 ± 0.045	0.153 ± 0.047	
$Q^2>4$ (GeV/c)^2, $20<\omega<100$	−	5.74 ± 0.46	1.66 ± 0.13	0.571 ± 0.071	0.166 ± 0.034	0.094 ± 0.026	0.047 ± 0.018
	+	5.64 ± 0.34	1.51 ± 0.12	0.704 ± 0.088	0.295 ± 0.055	0.126 ± 0.06	
$Q^2>0.3$ (GeV/c)^2, $\omega>100$	−	4.86 ± 0.13	1.71 ± 0.06	0.637 ± 0.035	0.223 ± 0.019	0.126 ± 0.015	0.048 ± 0.009
	+	4.99 ± 0.13	1.62 ± 0.06	0.521 ± 0.037	0.317 ± 0.052	0.07 ± 0.038	

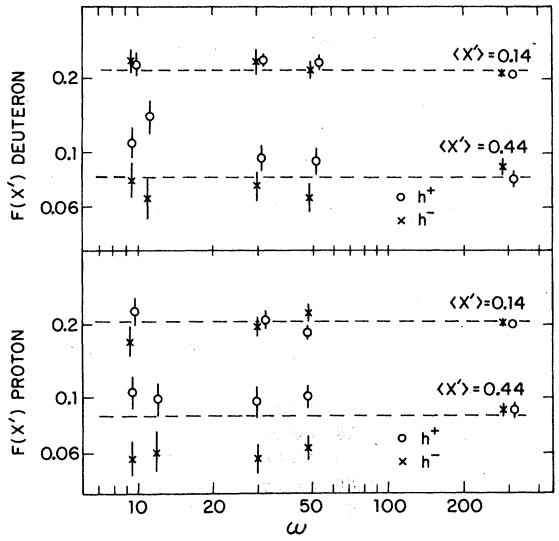

FIG. 10. $F(x')$ vs. ω for two values of x'. The dashed line is to guide the eye. The data are from the Q^2–ω ranges of Fig. 9(c).

Here $A = (E/\sigma)d^3\sigma/dp^3(p_T{}^2 = 0)$; b and $\mathfrak{N}$ are free parameters.

We chose this functional form for the fit because it has two properties: For small $p_T{}^2$ it goes as

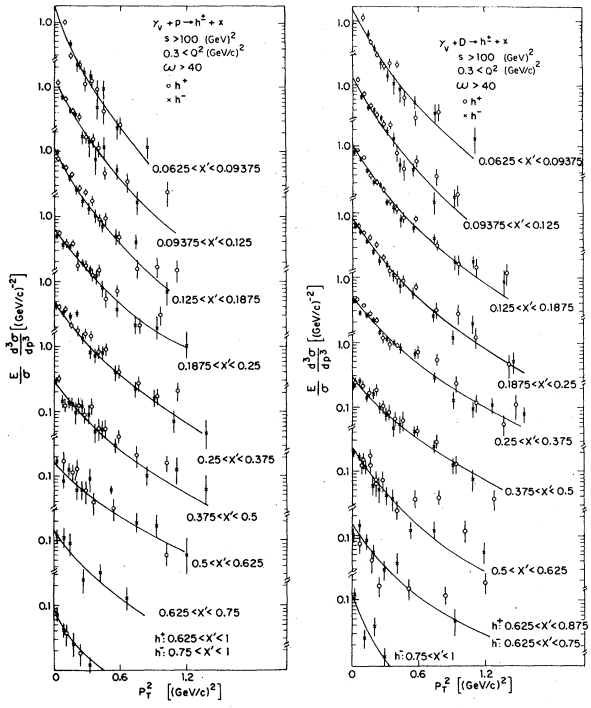

FIG. 11. $(E/\sigma)(d^3\sigma/dp^3)$ as a function of x' and $P_T{}^2$ for proton and deuteron. The solid lines are fits to the negative data.

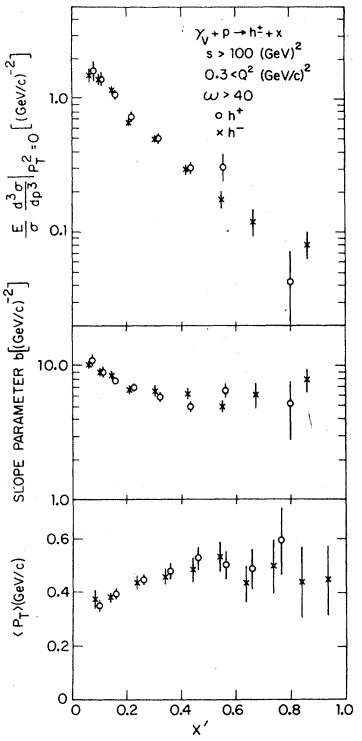

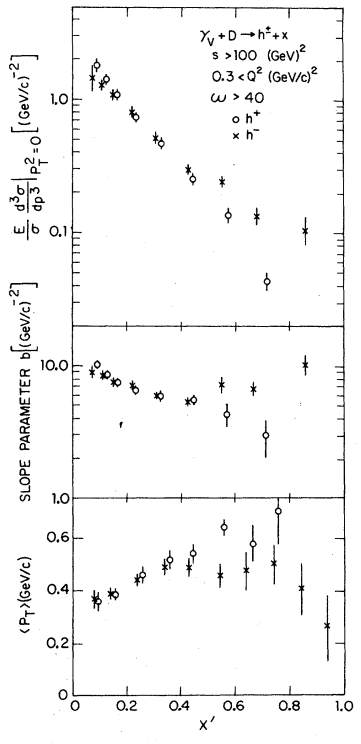

FIG. 12. Parameters of the fits to $(E/\sigma)(d^3\sigma/dp^3)$ as functions of x' and the average value of $\langle p_T \rangle$ as a function of x' directly measured.

TABLE VIII. Fits to the structure function $(E/\sigma)d^3\sigma/dp^3$ for proton and deuteron targets. Statistical errors only. There is an additional systematic error of ±4% and further errors for the positive hadrons are described in the text. $\mathfrak{M}$ is found to be 0.45 ± 0.05 GeV for $0.125 < x' < 0.1875$. The value of $\mathfrak{M}$ is fixed for the fits here at 0.45.

Formula: $$\frac{E}{\sigma}\frac{d^3\sigma}{dp^3} = A\left\{\exp\left(\frac{-2bp_T^2}{1+\left(1+\frac{p_T^2}{\mathfrak{M}^2}\right)^{1/2}}\right)\right\}$$

Target and muon kinematics	Charge	x' range	A $[(\mathrm{GeV}/c)^{-2}]$	b $[(\mathrm{GeV}/c)^{-2}]$
Proton				
$Q^2 > 0.3$ $(\mathrm{GeV}/c)^2$	−	$0.0625 < x' < 0.09375$	1.39 ±0.13	10.2 ±0.4
$\omega > 40$	+		1.61 ±0.28	11.2 ±1.0
$s > 100$ GeV^2	−	$0.09375 < x' < 0.125$	1.44 ±0.17	9.1 ±0.6
	+		1.40 ±0.11	8.9 ±0.5
	−	$0.125 < x' < 0.1875$	1.14 ±0.07	8.5 ±0.4
	+		1.05 ±0.06	7.8 ±0.3
	−	$0.1875 < x' < 0.25$	0.66 ±0.05	6.8 ±0.3
	+		0.73 ±0.05	6.8 ±0.3
	−	$0.25 < x' < 0.375$	0.47 ±0.03	6.4 ±0.3
	+		0.50 ±0.04	5.9 ±0.3
	−	$0.375 < x' < 0.5$	0.29 ±0.03	6.2 ±0.4
	+		0.30 ±0.03	5.0 ±0.4
	−	$0.5 < x' < 0.625$	0.175 ±0.025	5.0 ±0.5
	+		0.32 ±0.08	6.7 ±0.8
	−	$0.625 < x' < 0.75$	0.12 ±0.03	5.9 ±1.1
	+	$0.625 < x' < 1.0$	0.043 ±0.03	5.3 ±2.5
	−	$0.75 < x' < 1.0$	0.085 ±0.02	7.9 ±1.1
Deuteron				
$Q^2 > 0.3$ $(\mathrm{GeV}/c)^2$	−	$0.0625 < x' < 0.09375$	1.44 ±0.31	8.6 ±0.9
$\omega > 40$	+		1.78 ±0.23	10.3 ±0.8
$s > 100$ $(\mathrm{GeV})^2$	−	$0.09375 < x' < 0.125$	1.28 ±0.11	8.5 ±0.4
	+		1.40 ±0.08	8.8 ±0.38
	−	$0.125 < x' < 0.1875$	1.07 ±0.05	7.4 ±0.2
	+		1.07 ±0.05	7.4 ±0.24
	−	$0.1875 < x' < 0.25$	0.79 ±0.03	7.1 ±0.2
	+		0.74 ±0.04	6.7 ±0.26
	−	$0.25 < x' < 0.375$	0.51 ±0.02	6.1 ±0.1
	+		0.47 ±0.03	5.9 ±0.3
	−	$0.375 < x' < 0.5$	0.29 ±0.027	5.6 ±0.2
	+		0.25 ±0.02	5.5 ±0.3
	−	$0.5 < x' < 0.625$	0.24 ±0.02	7.3 ±0.4
	+		0.14 ±0.03	4.3 ±0.6
	−	$0.625 < x' < 0.75$	0.14 ±0.016	6.6 ±0.5
	+	$0.625 < x' < 0.875$	0.04 ±0.013	2.8 ±0.7
	−	$0.75 < x' < 1.0$	0.10 ±0.014	10.3 ±0.9

$A\exp(-bp_T^2)$ and for large p_T^2 it goes as $A\exp(-2b\mathfrak{M}p_T)$. These two behaviors are typical of hadron-hadron data in the respective ranges. The χ^2 per degree of freedom for the fits is consistent with statistical fluctuations only. The value of $\mathfrak{M}$ in the fit is determined by the low x' data only and is found to be 0.45 ± 0.05 GeV for the range $0.125 < x' < 0.1875$. Because of the beam deadener the statistics for the high-x' positive hadrons are too poor for the fit to be significant.

The need for two parameters b and $\mathfrak{M}$ to describe the transverse-momentum dependence of the data at low x' (the data are visibly consistent with one exponential for $x' \geq 0.2$) is consistent with the two-component slope behavior observed in other experiments.[33] These data do not go to low-enough x' for this effect to be observable if it persists at these energies.

The parameters of the fits are shown in Fig. 12 and listed in Table VIII. Figure 12 also shows the directly measured average transverse momentum of hadrons as a function of x' (which is listed

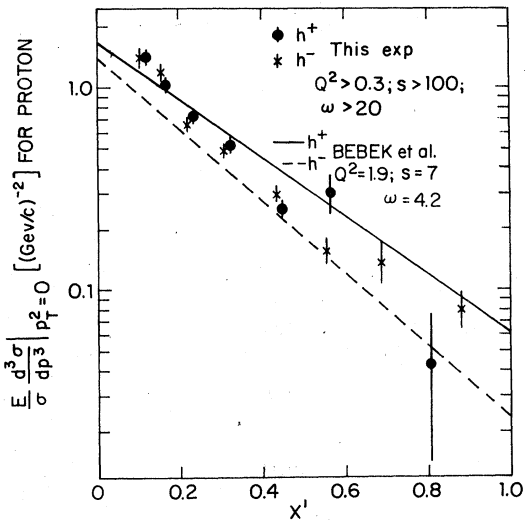

FIG. 13. Comparison between $(E/\sigma)(d^3\sigma/dp^3)$ for this experiment and the experiment of Bebek *et al.* (Ref. 34). The Q^2 ranges are in units of $(\mathrm{GeV}/c)^2$ and the s ranges are in units of GeV^2.

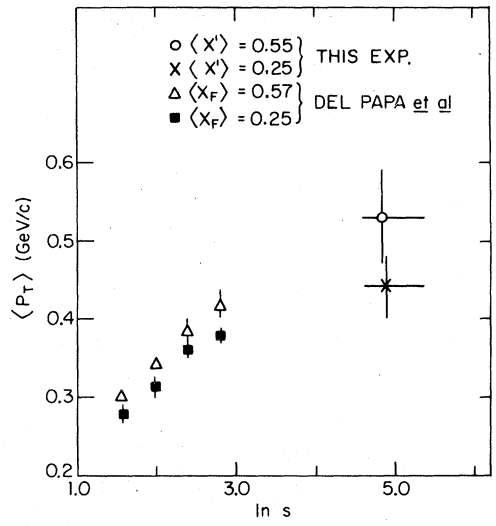

FIG. 15. Average transverse momentum for different x' or x_F ranges as a function of ln$s$. The data are from this experiment and that of del Papa *et al.* (Ref. 33).

in Table X). The parameter b and average transverse momentum show the seagull effect (the rise of average transverse momentum with x' or $-x'$) often seen in hadron interactions.

B. Comparisons with other electroproduction data

Figure 13 is a comparison of some of these data with lower-energy data of Bebek *et al.*[34] using the structure function $(E/\sigma)(d^3\sigma/dp^3)$. Figure 14 is a comparison of the structure function $F(x')$ between these data and the electroproduction data of Dakin *et al.*,[31] also at lower energy. In both cases the low- and high-energy data have approximately the same x dependence. However, while the high-energy structure functions are charge symmetric, the low-energy positive structure functions are larger than the negative structure functions. The Dakin *et al.* data are hadrons only

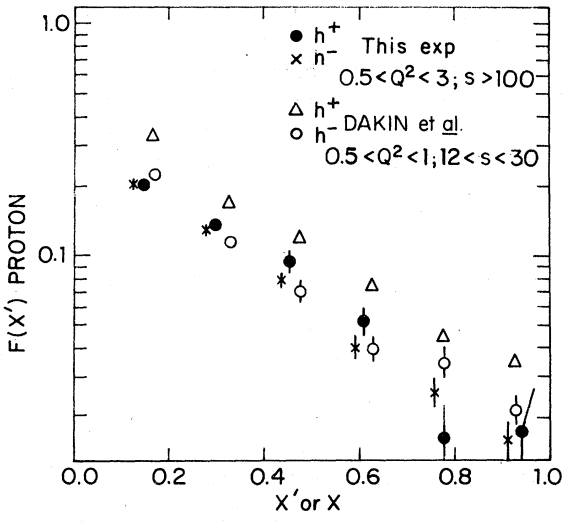

FIG. 14. Comparison of $F(x')$ between this experiment and the experiment of Dakin *et al.* (Ref. 31). The Q^2 ranges are in units of $(\mathrm{GeV}/c)^2$ and the s ranges are in units of GeV^2.

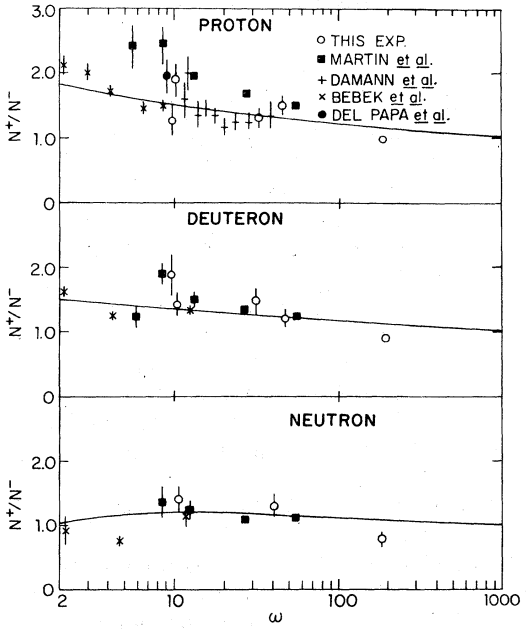

FIG. 16. Charge ratio for this and other experiments.

TABLE IX. Charge ratios for proton, deuteron and neutron targets ($0.3 < x' < 0.85$).

Target	Muon kinematics	N^+/N^- [a]	Systematic error
Proton	$3 < Q^2 < 6$ (GeV/c)^2, $5 < \omega < 20$	1.28 ± 0.21	± 0.07
	$Q^2 > 6$ (GeV/c)^2, $5 < \omega < 20$	1.90 ± 0.25	± 0.11
	$2 < Q^2 < 4$ (GeV/c)^2, $20 < \omega < 100$	1.51 ± 0.15	± 0.09
	$Q^2 > 4$ (GeV/c)^2, $20 < \omega < 100$	1.31 ± 0.17	± 0.08
	$Q^2 > 0.3$ (GeV/c)^2, $\omega > 100$	1.02 ± 0.08	± 0.06
Deuteron	$3 < Q^2 < 6$ (GeV/c)^2, $5 < \omega < 20$	1.90 ± 0.34	± 0.15
	$Q^2 > 6$ (GeV/c)^2, $5 < \omega < 20$	1.44 ± 0.18	± 0.12
	$2 < Q^2 < 4$ (GeV/c)^2, $20 < \omega < 100$	1.25 ± 0.15	± 0.10
	$Q^2 > 4$ (GeV/c)^2, $20 < \omega < 100$	1.48 ± 0.19	± 0.12
	$Q^2 > 0.3$ (GeV/c)^2, $\omega > 100$	0.91 ± 0.06	± 0.07
Neutron	$Q^2 > 3.0$ (GeV/c)^2, $5 < \omega < 20$	1.62 ± 0.30	± 0.29
	$Q^2 > 2.0$ (GeV/c)^2, $20 < \omega < 100$	1.24 ± 0.23	± 0.22
	$Q^2 > 0.3$ (GeV/c)^2, $\omega > 100$	0.79 ± 0.13	± 0.14

[a] Statistical errors only.

with significant numbers of protons, while the Bebek *et al.* data are pions only. Structure functions for hadrons produced by virtual photons of the same Q^2 appear to scale in the Feynman sense if averaged over charge.

Figure 15 is a comparison of the average transverse momentum of hadrons about the virtual-photon direction for this experiment and the muoproduction experiment of del Papa *et al.*,[33] also done at lower energies. The striking rise of the high x_F or x' average transverse momentum observed in the del Papa *et al.* experiment continues to higher energy going roughly as log s.

C. Comparison with the parton model

Figure 16 shows charge ratios for this and other experiments. These results are listed in Table IX. We have chosen 0.30 and 0.85 as the lower and upper x' cuts. The hydrogen and deuterium ratios measured here have systematic errors of $\pm 6\%$ and $\pm 8\%$, the neutron systematic error is $\pm 18\%$. There are some significant differences among the analyses. All experiments but this one and that of del Papa *et al.* report pion rather than hadron charge ratios. One process that substantially contributes to the difference between the pion and hadron ratios is forward proton production which decreases with energy.[35] Martin *et al.*[36] use a higher value of x_1', $x_1' = 0.4$, to define the charge ratio. Since the charge ratio appears to increase with x' (see Fig. 8), this may explain the higher values of N^+/N^- found by them. Martin *et al.*, del Papa *et al.*, and this experiment also remove ρ^0 mesons, while Bebek *et al.*[37] and Dammann *et al.*[38] do not. The latter experiments, however, begin at higher Q^2 and are unlikely to be affected by this. Despite these differences we believe that the data, taken together, support and ω-only dependence of the charge ratio. Note

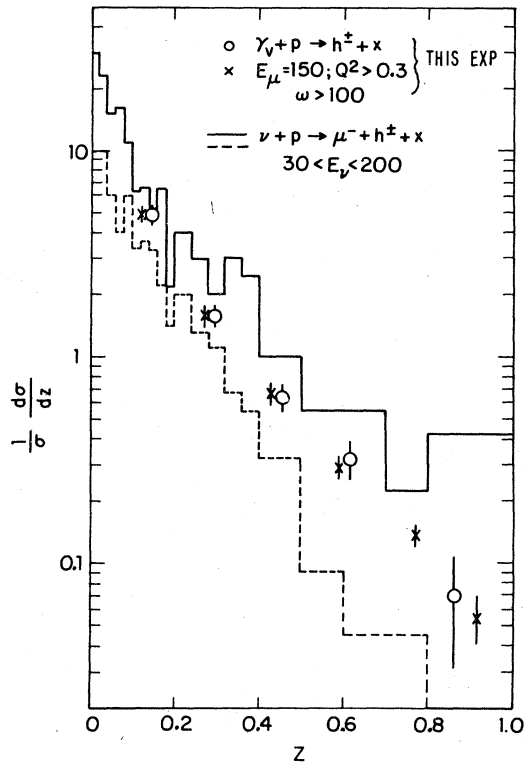

FIG. 17. Comparison of $(1/\sigma)(d\sigma/dz)$ for this experiment and neutrino experiments (Ref. 40); Q^2 is given in units of $(\mathrm{GeV}/c)^2$; E is given in units of GeV.

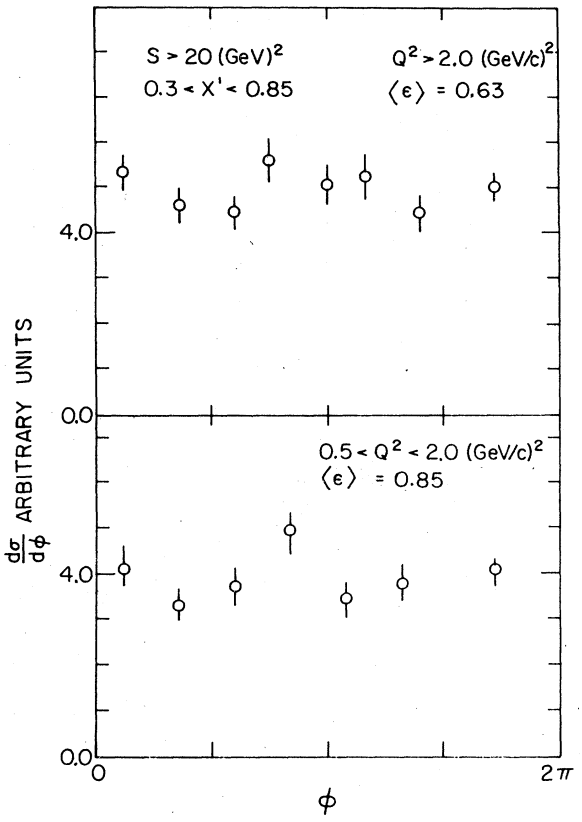

FIG. 18. Azimuthal distributions of hadrons about the direction of the virtual photon.

that the various experiments have very different Q^2 and ν ranges while giving comparable ω ranges.

We have fitted the hydrogen data with Dakin and Feldman's model, leaving out the Martin *et al.*, and del Papa *et al.* data. This yields a value of $\eta = 2.10 \pm 0.1$ with a χ^2 of 41.5 for 19 degrees of freedom. The predicted ratios for the deuteron and neutron using this value of η are shown on the graph.

A subsequent analysis by Martin and Osborne[39] gives $\eta = 2.8 \pm 0.3$. del Papa *et al.* find $\eta = 3.2 \pm 0.6$. Clearly, there are some inconsistencies in these results; they may be systematic in nature.

Figure 17 is a comparison of neutrino data[40] with the muoproduction data. We have used the structure function $(1/\sigma)(d\sigma/dz)$ rather than $F(x')$; this, however, does not affect the conclusions. We note the general agreement in shape and overall normalization with the difference being in the large charge asymmetry shown in the neutrino data compared with the negligible amount in the muon data. Note that the muon data averages the neutrino data as the naive quark model discussed before would predict.

The azimuthal distribution of hadrons about the virtual-photon direction is shown in Fig. 18. The data for proton and deuteron have been combined and the hadrons selected have $0.3 < x' < 0.85$. There is a suggestion of $\cos 2\phi$ dependence in the $Q^2 > 2.0$ $(\mathrm{GeV}/c)^2$ region. The coefficient of $\cos 2\phi$ in Eq. (6) expressed as a fraction of the constant terms is 0.115 ± 0.042 (0.100 ± 0.106) for $Q^2 > 2.0$ $(\mathrm{GeV}/c)^2$, $s > 20$ GeV^2, $\langle\epsilon\rangle = 0.84$ $[0.5 < Q^2 < 2.0$ $(\mathrm{GeV}/c)^2$, $s > 20$, $\langle\epsilon\rangle = 0.02]$. There is no significant $\cos\phi$ dependence. The small amount of azimuthal variation is consistent with quark-model expectations and may be significant for AFGT. This small variation also justifies our assumption of no ϕ dependence in the estimation of structure functions integrated over ϕ.

In the quark model νW_2 and the structure function $F(x')$ both describe the decomposition of an initial particle into a set of secondary particles. There may be reciprocity here, as the former is that of a hadron decomposed into quarks, and the latter is the reverse. Further, νW_2 and $F(x')$ have the same approximate form in terms of the momentum fraction x_B or x'. A better choice

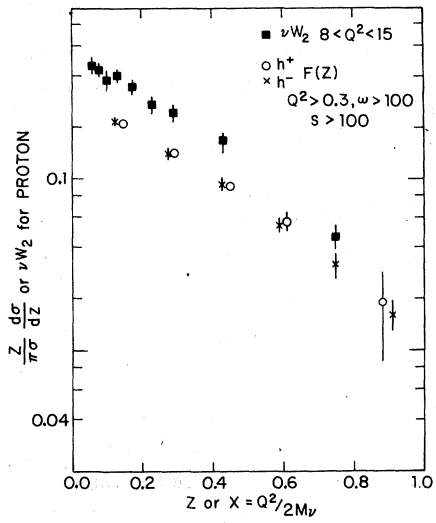

FIG. 19. Comparison of νW_2 for proton (Ref. 10) with hadron structure function $F(z)$ for proton. All data are from this experiment. Q^2 is given in units of $(\mathrm{GeV}/c)^2$; s is given in units of GeV^2.

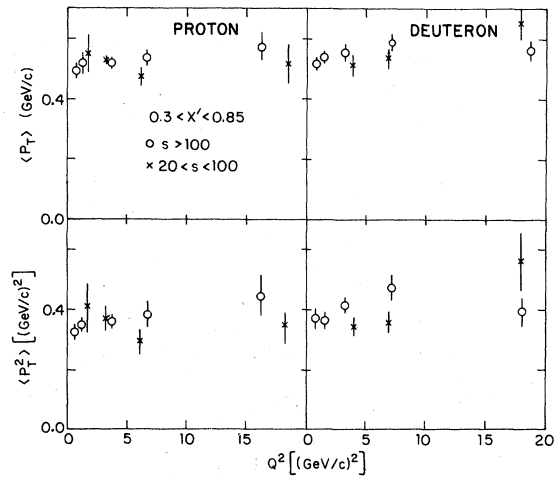

FIG. 21. Moments of the p_T distribution in the photon hemisphere as functions of Q^2.

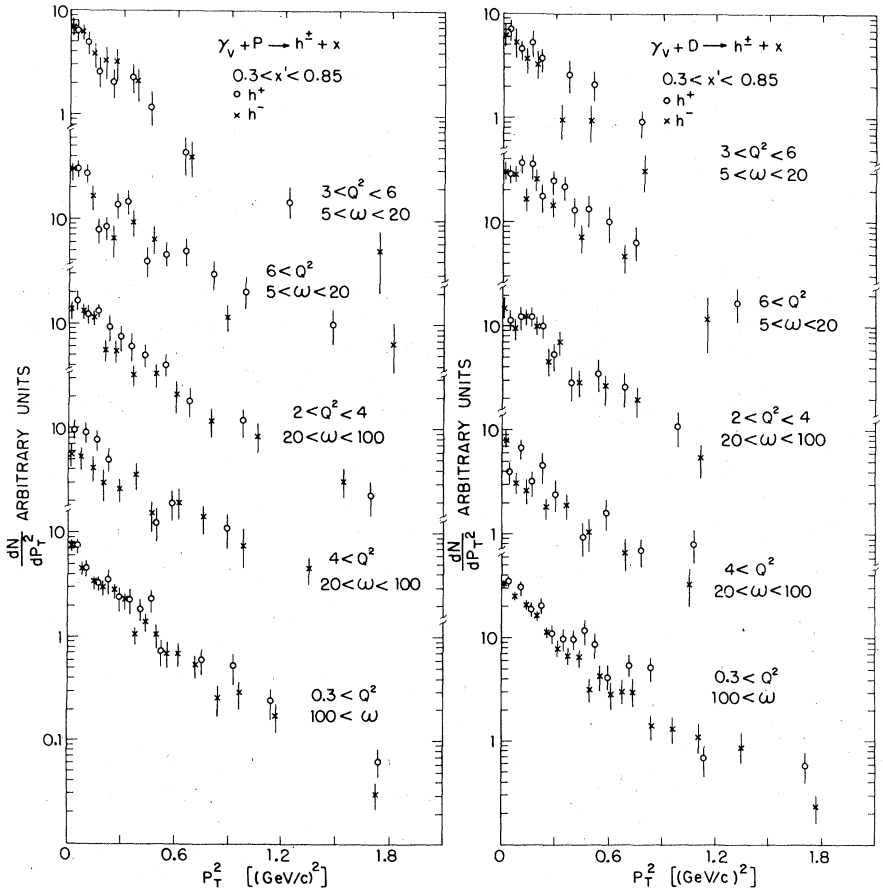

FIG. 20. Forward transverse-momentum distributions as a function of Q^2 and ω. The vertical scales are arbitrary even between positive and negative charges for the same Q^2 and ω. The Q^2 ranges are given in $(\mathrm{GeV}/c)^2$.

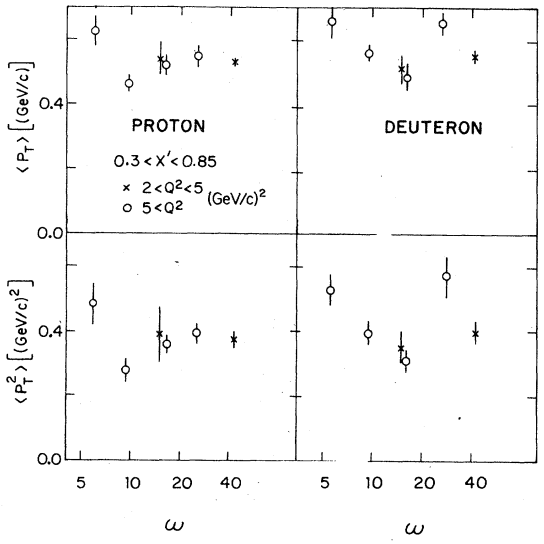

FIG. 22. Moments of the p_T distributions in the photon hemisphere as functions of ω.

of variable in the case of the hadron structure function is z defined in Eq. (6). This is a true invariant analogous to $x_B = Q^2/2M\nu$ used for νW_2. Figure 19 shows the two structure functions. It should be noted that $F(x')$ is dimensionless, whereas νW_2 is in units of charge squared. It is striking that the shape of the two distributions is quite similar. There are some predictions for this behavior.[41]

D. Hadron-transverse-momentum dependence

The transverse-momentum distribution of positive and negatively charged hadrons, for our standard Q^2-ω ranges, is shown in Fig. 20. The data have $0.3 < z < 0.85$, and the normalization is arbitrary even between the opposite charges in the same muon bin. Figures 21 and 22 show the first and second moments, $\langle P_T \rangle$ and $\langle P_T{}^2 \rangle$ (defined in Table III and listed in Table X) as functions of s and Q^2 or Q^2 and ω. The typical values of $\langle P_T \rangle$ is about 0.35 $(\mathrm{GeV}/c)^2$ of which the previously estimated radiative contribution, 0.01 $(\mathrm{GeV}/c)^2$ is less than 3%. There is no suggestion of any dependence of these data on the muon scattering variables.

Because of their weak Q^2 dependence, the effects predicted by AFGT are too small to have been seen clearly in our data. Such effects may also be masked by the contributions to the transverse momentum of the final-state hadron interactions. The same reservation applies when we compare to the Q^2 dependence expected from the photon's hadronic aspect. The simplest Q^2 dependence is stronger in this case than in AFGT, and the lack of any change in $\langle p_T \rangle$ or $\langle p_T{}^2 \rangle$ over the range $0.5\ (\mathrm{GeV}/c)^2 < Q^2 < 20\ (\mathrm{GeV}/c)^2$ is striking and perhaps significant to the hadronic photon viewpoint.

E. Jets

Hanson[22] has analyzed the inclusive structure of hadron jets in e^+e^- annihilation. Using events

TABLE X. Transverse-momentum moments for proton and deuteron targets.

Target	Muon kinematics	Hadron kinematics	Charge	$\langle p_T \rangle$ (GeV/c)	$\langle p_T{}^2 \rangle$ [(GeV/c)^2]
Proton	$Q^2 > 0.3$ (GeV/c)^2	$0.06 < x' < 0.1$	−	0.37 ± 0.04	
	$\omega > 40$		+	0.35 ± 0.02	
	$s > 100$ (GeV)^2	$0.1 < x' < 0.2$	−	0.38 ± 0.02	
			+	0.39 ± 0.02	
		$0.2 < x' < 0.3$	−	0.44 ± 0.03	
			+	0.44 ± 0.03	
		$0.3 < x' < 0.4$	−	0.46 ± 0.04	
			+	0.48 ± 0.04	
		$0.4 < x' < 0.5$	−	0.49 ± 0.05	
			+	0.53 ± 0.05	
		$0.5 < x' < 0.6$	−	0.53 ± 0.06	
			+	0.50 ± 0.07	
		$0.6 < x' < 0.7$	−	0.43 ± 0.08	
			+	0.48 ± 0.07	
		$0.7 < x' < 0.8$	−	0.50 ± 0.10	
			+	0.60 ± 0.13	
		$0.8 < x' < 0.9$	−	0.44 ± 0.13	
			+	...	
		$0.9 < x' < 1.0$	−	0.46 ± 0.13	
			+	...	

TABLE X. *(Continued)*.

Target	Muon kinematics	Hadron kinematics	Charge	$\langle p_T \rangle$ (GeV/c)	$\langle p_T^2 \rangle$ [(GeV/c)^2]
Deuteron	$Q^2 > 0.3$ (GeV/c)^2	$0.06 < x' < 0.1$	$-$	0.37 ± 0.03	
	$\omega > 40$		$+$	0.36 ± 0.03	
	$s > 100$ (GeV)^2	$0.1 < x' < 0.2$	$-$	0.39 ± 0.02	
			$+$	0.38 ± 0.02	
		$0.2 < x' < 0.3$	$-$	0.44 ± 0.02	
			$+$	0.46 ± 0.02	
		$0.3 < x' < 0.4$	$-$	0.49 ± 0.03	
			$+$	0.52 ± 0.03	
		$0.4 < x' < 0.5$	$-$	0.49 ± 0.04	
			$+$	0.54 ± 0.04	
		$0.5 < x' < 0.6$	$-$	0.45 ± 0.05	
			$+$	0.64 ± 0.06	
		$0.6 < x' < 0.7$	$-$	0.48 ± 0.07	
			$+$	0.58 ± 0.07	
		$0.7 < x' < 0.8$	$-$	0.51 ± 0.08	
			$+$	0.70 ± 0.11	
		$0.8 < x' < 0.9$	$-$	0.41 ± 0.10	
			$+$	...	
		$0.9 < x' < 1.0$	$-$	0.27 ± 0.14	
			$+$	...	
Proton	$20 < s < 100$ (GeV)^2				
	$1.0 < Q^2 < 2.0$ (GeV/c)^2	$0.3 < x' < 0.85$	$+/-$	0.57 ± 0.05	0.44 ± 0.08
	$2.0 < Q^2 < 5.0$ (GeV/c)^2			0.53 ± 0.02	0.38 ± 0.03
	$5.0 < Q^2 < 10.0$ (GeV/c)^2			0.47 ± 0.02	0.29 ± 0.03
	$Q^2 > 10.0$ (GeV/c)^2			0.50 ± 0.04	0.35 ± 0.06
	$s > 100$ (GeV)^2				
	$0.5 < Q^2 < 1.0$ (GeV/c)^2			0.50 ± 0.02	0.33 ± 0.02
	$1.0 < Q^2 < 2.0$ (GeV/c)^2			0.53 ± 0.02	0.36 ± 0.02
	$2.0 < Q^2 < 5.0$ (GeV/c)^2			0.53 ± 0.02	0.37 ± 0.02
	$5.0 < Q^2 < 10.0$ (GeV/c)^2			0.53 ± 0.02	0.38 ± 0.02
	$Q^2 > 10.0$ (GeV/c)^2			0.58 ± 0.04	0.45 ± 0.06
Deuteron	$20 < s < 100$ (GeV)^2				
	$3.0 < Q^2 < 5.0$ (GeV/c)^2	$0.3 < x' < 0.85$	$+/-$	0.52 ± 0.03	0.35 ± 0.03
	$5.0 < Q^2 < 10.0$ (GeV/c)^2			0.54 ± 0.02	0.36 ± 0.03
	$Q^2 > 10.0$ (GeV/c)^2			0.65 ± 0.05	0.56 ± 0.08
	$s > 100$ (GeV)^2				
	$0.5 < Q^2 < 1.0$ (GeV/c)^2			0.52 ± 0.02	0.38 ± 0.02
	$1.0 < Q^2 < 2.0$ (GeV/c)^2			0.54 ± 0.02	0.38 ± 0.02
	$2.0 < Q^2 < 5.0$ (GeV/c)^2			0.56 ± 0.02	0.42 ± 0.02
	$5.0 < Q^2 > 10.0$ (GeV/c)^2			0.59 ± 0.03	0.48 ± 0.04
	$Q^2 > 10.0$ (GeV/c)^2			0.57 ± 0.03	0.40 ± 0.04
Proton	$2.0 < Q^2 < 5.0$ (GeV/c)^2				
	$12 < \omega < 20$	$0.3 < x' < 0.85$	$+/-$	0.55 ± 0.04	0.40 ± 0.07
	$\omega > 20$			0.53 ± 0.02	0.38 ± 0.02
	$Q^2 > 5.0$ (GeV/c)^2				
	$5 < \omega < 7$			0.61 ± 0.05	0.49 ± 0.07
	$7 < \omega < 12$			0.46 ± 0.03	0.29 ± 0.03
	$12 < \omega < 20$			0.51 ± 0.02	0.36 ± 0.03
	$\omega > 20$			0.54 ± 0.03	0.39 ± 0.03
Deuteron	$2.0 < Q^2 < 5.0$ (GeV/c)^2				
	$7 < \omega < 12$	$0.3 < x' < 0.85$	$+/-$	0.48 ± 0.10	0.26 ± 0.10
	$12 < \omega < 20$			0.51 ± 0.04	0.34 ± 0.05
	$\omega > 20$			0.56 ± 0.02	0.41 ± 0.02
	$Q^2 > 5.0$ (GeV/c)^2				
	$5 < \omega > 7$			0.66 ± 0.03	0.53 ± 0.06
	$7 < \omega < 12$			0.56 ± 0.03	0.39 ± 0.04
	$12 < \omega < 20$			0.49 ± 0.02	0.31 ± 0.03
	$\omega > 20$			0.66 ± 0.04	0.58 ± 0.06

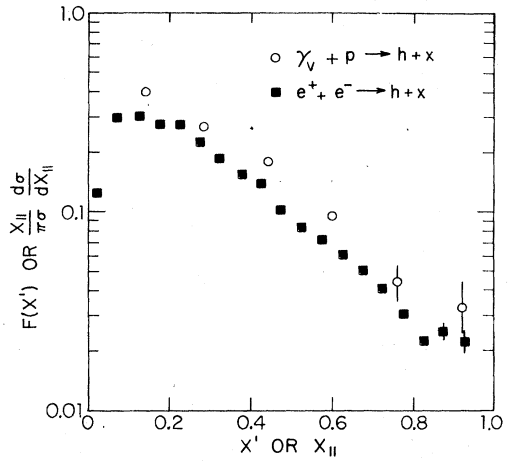

FIG. 23. Comparison of structure functions for muon scattering and e^+e^- annihilation. The muon data have $s > 100$ GeV^2 and $0.5 \leq Q^2 \leq 3.00$ (GeV/c)^2. The e^+e^- data are from Ref. 20 and have $s = 56$ GeV^2.

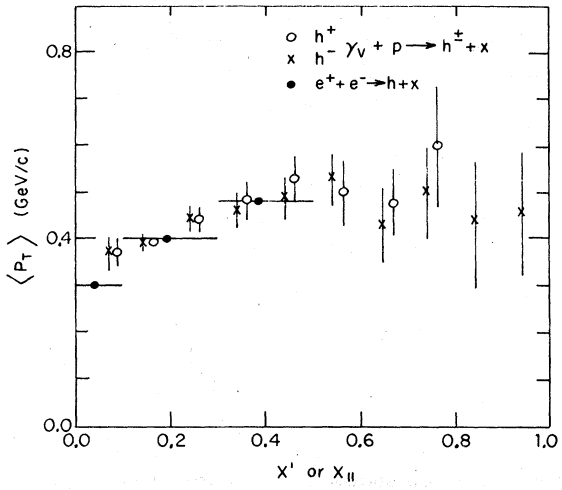

FIG. 25. Average transverse momentum with respect to x' or x_{II} for muon scattering and e^+e^- data. The muon data are from Table X. The e^+e^- data are from Ref. 20.

in which the axis of one of the back-to-back jets could be simply inferred and correcting the data with the aid of a Monte Carlo jet model she has obtained the inclusive hadron structure functions for the other jet in the event. She excluded heavy-lepton events and demonstrated that there was little bias in the method. Figure 23 is a comparison of the longitudinal structure function for charged hadrons $[F^+(x') + F^-(x')]$ from this experiment and the nearly equivalent structure function $(x_{II}/\pi\sigma)(d\sigma/dx_{II})$ for one of the jets in e^+e^- annihilation, where x_{II} is the scaled momentum component of a hadron along the jet axis: $x_{II} = 2p_{II}/E_{c.m.}$. ($E_{c.m.}$ is the energy of an incident electron.) In the s region where the data overlap, the two distributions have the same shape; however, the

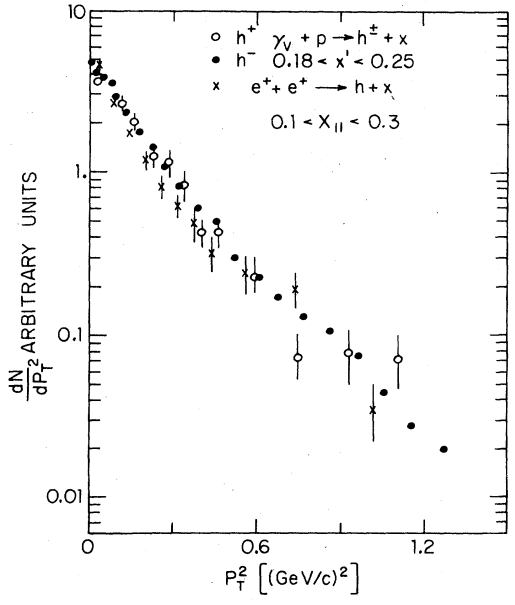

FIG. 24. Comparison of transverse-momentum distributions about the virtual photon for muon scattering and about the jet axis for e^+e^- annihilation. The muon data are from Fig. 11. The e^+e^- are from Ref. 20.

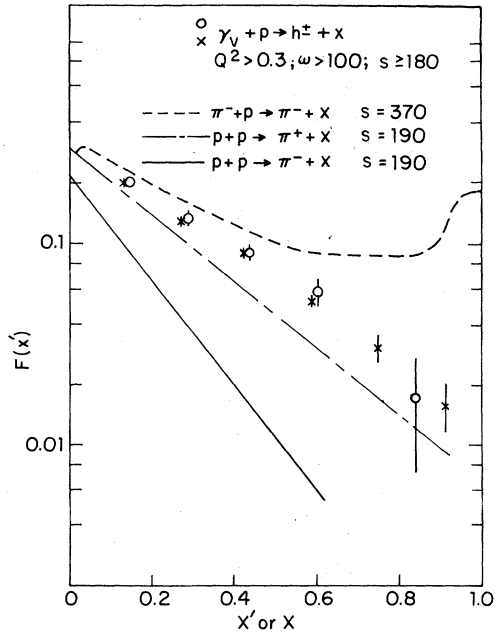

FIG. 26. Comparison of $F(x')$ for this experiment with corresponding structure functions for hadron experiments (Ref. 43). Q^2 is given in units of (GeV/c)^2; s is given in units of GeV^2.

results from muoproduction are higher. This indicates that in muoproduction more of the total available energy is put into charged hadrons. This is a natural consequence of the decrease, as energy increases, in the fraction of energy in charged hadrons in e^+e^- annihilation[42] and may be a result of the production of charmed final states.

Figure 24 compares the hadron transverse-momentum distribution about the virtual-photon direction in muoproduction with that about the jet axis in e^+e^- annihilation. The normalizations are arbitrary. The shape agreement is excellent. Figure 25 shows $\langle P_T \rangle$ as a function of x' or $x_{\parallel}$ for the two processes again with excellent agreement.

Insofar as the hadrons in e^+e^- annihilation exhibit the collimation expected of jet behavior, muoproduction shows the behavior predicted by the jet hypothesis.

F. Comparisons with hadron data

We have already noted some similarities between the muoproduction data and hadron-hadron inclusive spectra. These were Feynman scaling, the seagull effect, and average transverse momentum of the muoproduced hadrons. Figure 26 shows a comparison between the longitudinal structure function observed in muoproduction and that for typical hadron-proton reactions.[43] As x' decreases, the values of the structure function are converging, consistent with the rough invariance of hadron multiplicity among different reactions. At high x' only the $\pi^- + p \to \pi^- + p$ reaction, which has a leading-particle effect, produces more hadrons per interaction than the virtual photon. Figure 27 shows a comparison for the rapidity distributions observed in muoproduction and hadron reactions.[44] The shapes of the distributions are similar with the virtual-photon hadrons reaching rapidities less extreme than the hadrons in the leading particle channel, and more extreme than those in the unlike sign particle channel. The production of hadrons by virtual photons is not grossly different from that by hadrons.

VII. CONCLUSIONS

We have measured the inclusive hadron spectra in the photon-fragmentation hemisphere for muon scattering by protons and deuterons at a beam energy of 147 GeV. The data show no strong dependence on the variables that describe muon scattering and agree with lower-energy data. We find no disagreement with the predictions of the parton model even in the previously unmeasured kinematic regions. There is also no variation in the average transverse momentum of muoproduced hadrons with respect to the virtual-photon direction as a function of Q^2 or ω. The data exhibit a jet behavior consistent with that observed in e^+e^- annihilation and are consistent with the jet hypothesis. The general character of the hadrons produced in the interaction of virtual photons with nucleons is very similar to that for hadrons produced in hadron-nucleon interactions.

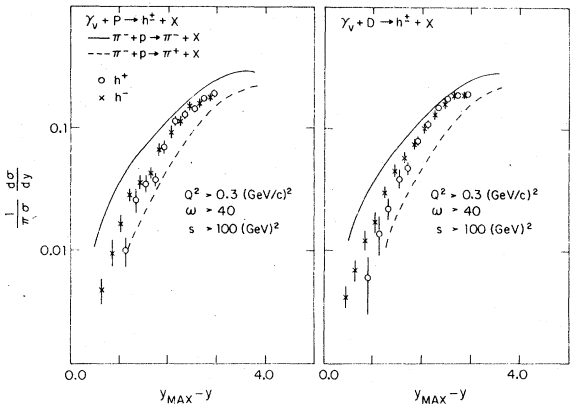

FIG. 27. Comparison of rapidity distribution produced by muon and hadron interactions. The hadron data are from Ref. 44.

ACKNOWLEDGMENTS

Many people, beyond the authors of this paper, made essential contributions to this experiment. At the Enrico Fermi Institute, T. Nunamaker, B. Norton, R. Gabriel, and R. Armstrong designed pieces of the apparatus, W. Nakagawa, F. Quinn, K. Burns, B. Grummon, and D. Turner fabricated and maintained the same. At Harvard, E. Sadowski designed the large 2×6-m chambers, H. Weedon designed the high-voltage pulsers for these chambers, and R. Burns, R. Haggerty, and J. O'Kane played a major role in constructing this chamber system. At Oxford, P. Burton mounted the hodoscopes and was an enthusiastic helper in any arduous task that came to hand, while Leslie Jones and John MacAllister solved many computing problems with great efficiency. We thank all these invaluable people as well as others who made the experiment possible.

This research was supported by the National Science Foundation under Contract No. PHY-71-02186-A05, by the U. S. Department of Energy under Contracts No. EY-76-C-02-3064 and No. E(11-1)-1195, and by the Science Research Council (United Kingdom).

*Present address: CERN, 1211 Geneva 23, Switzerland.
†Present address: Massachusetts General Hospital, Boston, Massachusetts 02155.
‡Present address: Nevis Laboratory, Columbia University, New York, N. Y. 10027.
§Present address: Department of Physics, Virginia Polytechnic Institute and State University, Blacksburg, Va. 24061.
‖Present address: Los Alamos Scientific Laboratory, Los Alamos, N. M. 87545.
¶Present address: Michigan State University, East Lansing, Michigan 48823.
**Present address: Fermilab, Batavia, Illinois 60510.
††Present address: Physics Department, University of California, Santa Barbara, California 93106.
‡‡Present address: Hanson Laboratory, Stanford University, Stanford, California 94305.
§§Present address: Physics Department, University of Maryland, College Park, Maryland 20742.

[1]W.H.K. Panofsky, in *Proceedings of the Fourteenth International Conference on High Energy Physics, Vienna, 1968,* edited by J. Prentki and J. Steinberger (CERN, Geneva, 1968), pp. 36-37. The experimental group was E. Bloom, D. Coward, H. deStaebler, I. Drees, J. Litt, G. Miller, L. Mo, R. Taylor, M. Breidenbach, J. Friedman, G. Hartmann, H. Kendall, and S. Loken.

[2]J. D. Bjorken, Phys. Rev. 179, 1547 (1969).

[3]R. P. Feynman, *Photon-Hadron Interactions* (Benjamin, New York, 1972).

[4]J. D. Bjorken and E. A. Paschos, Phys. Rev. 185, 1975 (1969).

[5]A. Entenberg, H. Jostlein, I. Kostoulas, A. C. Melissinos, L. M. Lederman, P. Limon, M. May, P. Rapp, H. Gittleson, T. Kirk, M. Murtagh, M. J. Tanenbaum, J. Sculli, T. White, and T. Yamanouchi, Phys. Rev. Lett. 32, 486 (1974); I. Kostoulas, A. Entenberg, H. Jostlein, A. C. Melissinos, L. M. Lederman, P. Limon, M. May, P. Rapp, H. Gittleson, T. Kirk, M. Murtagh, M. J. Tanenbaum, J. Sculli, T. White, and T. Yamanouchi, Phys. Rev. Lett. 32, 489 (1974).

[6]W. A. Loomis, H. S. Matis, H. L. Anderson, V. K. Bharadwaj, N. E. Booth, R. M. Fine, W. R. Francis, B. A. Gordon, R. H. Heisterberg, R. G. Hicks, T. B. W. Kirk, G. I. Kirkbride, L. W. Mo, L. C. Myrianthopoulos, F. M. Pipkin, S. H. Pordes, T. W. Quirk, W. D. Shambroom, A. Skuja, L. J. Verhey, W. S. C. Williams, Richard Wilson, and S. C. Wright, Phys. Rev. Lett. 35, 1483 (1975).

[7]H. L. Anderson, V. K. Bharadwaj, N. E. Booth, R. M. Fine, W. R. Francis, B. A. Gordon, R. H. Heisterberg, R. G. Hicks, T. B. W. Kirk, G. I. Kirkbride, W. A. Loomis, H. S. Matis, L. W. Mo, L. C. Myrianthopoulos, F. M. Pipkin, S. H. Pordes, T. W. Quirk, W. D. Shambroom, A. Skuja, L. J. Verhey, W. S. C. Williams, Richard Wilson, and S. C. Wright, Phys. Rev. Lett. 36, 1422 (1976).

[8]Howard S. Matis, Ph.D. thesis, University of Chicago, 1976 (unpublished).

[9]H. L. Anderson, V. K. Bharadwaj, N. E. Booth, R. M. Fine, W. R. Francis, B. A. Gordon, R. H. Heisterberg, R. G. Hicks, T. B. W. Kirk, G. I. Kirkbride, W. A. Loomis, H. S. Matis, L. W. Mo, L. C. Myrianthopoulos, F. M. Pipkin, S. H. Pordes, T. W. Quirk, W. D. Shambroom, A. Skuja, L. J. Verhey, W. S. C. Williams, Richard Wilson, and S. C. Wright, Phys. Rev. Lett. 37, 4 (1976).

[10]H. L. Anderson, V. K. Bharadwaj, N. E. Booth, R. M. Fine, W. R. Francis, B. A. Gordon, R. H. Heisterberg, R. G. Hicks, T. B. W. Kirk, G. I. Kirkbride, W. A. Loomis, H. S. Matis, L. W. Mo, L. C. Myrianthopoulos, F. M. Pipkin, S. H. Pordes, T. W. Quirk, W. D. Shambroom, A. Skuja, L. J. Verhey, W. S. C. Williams, Richard Wilson, and S. C. Wright, Phys. Rev. Lett. 38, 1450 (1977).

[11]V. K. Bharadwaj, thesis, Oxford University, 1977 (unpublished).

[12]B. A. Gordon, thesis, Harvard University, 1978 (unpublished).

[13]I. Kirkbride, thesis, Oxford University, 1976 (unpublished).

[14]S. H. Pordes, thesis, Harvard University, 1976 (unpublished).

[15]R. H. Heisterberg, thesis, University of Chicago, 1976 (unpublished).

[16]J. T. Dakin and G. J. Feldman, Phys. Rev. D 8, 2862 (1973).

[17]F. Ravndal, Phys. Lett. 43B, 301 (1973).

[18]D. J. Gross and F. Wilczek, Phys. Rev. D 8, 3633 (1973); 9, 980 (1974); H. Georgi and H. D. Politzer, *ibid.* 416 (1974); H. D. Politzer, Phys. Rep. 14C, 129 (1974).

[19]I. Hinchliffe and C. H. Llewellyn Smith, Phys. Lett. 66B, 281 (1977); J. B. Kogut, *ibid.* 65B, 377 (1976).

[20]R. P. Feynman, R. D. Field, and G. C. Fox, Phys. Rev. D 18, 3320 (1978). R. D. Field and R. P. Feynman, *ibid.* 15, 2590 (1977).

[21]A series of lectures on this point of view was given by J. D. Bjorken, in ***Deep Hadronic Structure and the New Particles***, Proceedings of Summer Institute on Particle Physics, 1975, edited by Martha C. Zipf (SLAC, Stanford, 1975), pp. 85–118.

[22]G. Hanson, in ***Gauge Theories and Leptons***, proceedings of the XIII Rencontre de Moriond, Les Arcs, France, 1978, edited by J. Trân Thanh Vân (Editions Frontières, Gif-sur-Yvette, 1978), pp. 15–42.

[23]Sphericity S: $S = 3(\sum_i P_{Ti}{}^2)_{\min}/2\sum_i \mathbf{P}_i{}^2$. The P_{Ti} are with respect to the direction that minimizes S.

[24]T. H. Bauer, R. D. Spital, D. R. Yennie, and F. M. Pipkin, Rev. Mod. Phys. 50, 261 (1978).

[25]R. P. Feynman, Phys. Rev. Lett. 23, 1415 (1969).

[26]H. Cheng and T. T. Wu, Phys. Rev. 183, 1324.

[27]W. R. Francis, H. L. Anderson, V. K. Bharadwaj, N. E. Booth, R. M. Fine, B. A. Gordon, R. H. Heisterberg, R. G. Hicks, T. B. W. Kirk, G. I. Kirbride, W. A. Loomis, H. S. Matis, L. W. Mo, L. C. Myrianthopoulos, F. M. Pipkin, S. H. Pordes, T. W. Quirk, W. D. Shambroom, A. Skuja, L. J. Verhey, W. S. C. Williams, Richard Wilson, and S. C. Wright, Phys. Rev. Lett. 38, 633 (1977).

[28]L. W. Mo and Y. Tsai, Rev. Mod. Phys. 41, 247 (1969).

[29]Y. Tsai, SLAC Report No. SLAC-PUB-848, 1971 (unpublished).

[30]A. Bodek, thesis, Massachusetts Institute of Technology, 1977 (unpublished).

[31]J. T. Dakin, G. J. Feldman, M. L. Perl, and W. T. Toner, Phys. Rev. D 10, 1401 (1974).

[32]P. H. Garbincius, K. Berkelman, B. Gibbard, J. S. Kluger, P. Wanderer, and A. J. Sadoff, Phys. Rev. Lett. 32, 328 (1974). A. J. Sadoff, K. Berkelman, P.

H. Garbincius, B. Gibbard, J. S. Klinger, and P. Wanderer, Phys. Rev. Lett. 32, 955 (1974).
[33]C. del Papa, D. Dorfan, S. M. Flatté, C. A. Heusch, B. Liberman, H. Meyer, L. Moss, T. Schalk, A. Seiden, K. Bunnell, M. Duoug-Van, R. Mozley, A. Odian, F. Villa, and L. C. Wang, Phys. Rev. D 15, 2425 (1977).
[34]C. J. Bebek, A. Brownman, C. N. Brown, K. M. Hanson, R. V. Kline, D. Larson, F. M. Pipkin, S. W. Raither, A. Silverman, and L. K. Sisterson, Phys. Rev. Lett. 37, 1525 (1976).
[35]C. J. Bebek, A. Brownman, C. N. Brown, K. M. Hanson, R. V. Kline, D. Larson, F. M. Pipkin, S. W. Raither, A. Silverman, and L. K. Sisterson, Phys. Rev. Lett. 37, 1320 (1976).
[36]J. F. Martin, C. Bolon, R. C. Lanza, D. Luckey, L. S. Osborne, D. G. Roth, G. J. Feldman, G. Hanson, D. E. Lyon, M. L. Perl, T. Pun, and J. T. Dakin, Phys. Lett. 65B, 483 (1976).
[37]C. J. Bebek, C. N. Brown, R. V. Kline, F. M. Pipkin, S. W. Raither, L. K. Sisterson, A. Browman, K. M. Hanson, D. Larson, and A. Silverman, Phys. Rev. D 16, 1986 (1977).
[38]I. Damman, C. Driver, K. Héinloth, G. Hofmann, F. Janata, P. Karow, D. Lüke, D. Schmidt, and G. Sprecht, Nucl. Phys. B54, 381 (1973).
[39]J. F. Martin and L. S. Osborne, Phys. Rev. Lett. 38, 1193 (1977).
[40]J. P. Berge *et. al.*, Fermilab Report No. Fermilab Pub 75/84-Exp. 7300.045 (unpublished). See also J. Bell *et al.*, Phys. Rev. D 19, 1 (1979).
[41]D. C. Fetzer and H. Schlereth, Nuovo Cimento 31, 65 (1976). This has calculations based on reciprocity as well as a discussion of the theoretical basis for reciprocity.
[42]G. Hanson, in *Proceedings of the Seventh International Colloquium on Multiparticle Production, Tutzing, Munich, 1976*, edited by J. Benecke *et. al.* (Max-Planck-Institut, Munich, 1976), p. 313; in *Proceedings of the Eighteenth International Conference on High Energy Physics, Tbilisi, 1976*, edited by N. N. Bogolubov *et al.* (JINR, Dubna, U.S.S.R., 1977), Vol. II, p. B1.
[43]J. Whitmore, Phys. Rep. 10C, 273 (1974); W. Morris, B. Y. Ou, D. L. Parker, G. A. Smith, J. Whitmore, L. Voyvodic, R. Walker, R. Yaari, E. W. Anderson, H. B. Crawley, W. J. Kernan, F. Ogino, R. G. Glasser, D. G. Hill, G. McClellan, H. L. Price, B. Sechi-Zorn, G. A. Snow, F. Surcek, W. D. Shepard, J. M. Bishop, N. N. Biswas, N. M. Cason, E. D. Fokitis, and V. P. Kenney, Phys. Lett. 56B, 395 (1975).
[44]V. P. Kenney *et al.*, Fermilab Bubble Chamber Spectrometer Documentation, Fermilab Bubble Chamber Symposium, 1975, (unpublished) page A93.